Powder Technology 372 (2020) 372–393

Contents lists available at ScienceDirect

Powder Technology

journal homepage: www.elsevier.com/locate/powtec

Computationally inexpensive simulation of agglomeration in spray drying while preserving structure related information using CFD

Hasan Jubaer [a], Sepideh Afshar [a], Serge Mejean [b], Romain Jeantet [b], Jie Xiao [c], Xiao Dong Chen [c], Cordelia Selomulya [a,d], Meng Wai Woo [a,e,*]

[a] Faculty of Engineering, Department of Chemical Engineering, Monash University, VIC, Australia
[b] UMR 1253 STLO, INRA, Agrocampus Ouest, F-35042 Rennes, France
[c] Suzhou Key Laboratory of Green Chemical Engineering, School of Chemical and Environmental Engineering, College of Chemistry, Chemical Engineering and Materials Science, Soochow University, Suzhou, Jiangsu, China
[d] School of Chemical Engineering, The University of New South Wales (UNSW), Sydney, NSW 2052, Australia
[e] Department of Chemical and Materials Engineering, The University of Auckland, New Zealand

ARTICLE INFO

Article history:
Received 25 February 2020
Received in revised form 13 May 2020
Accepted 29 May 2020
Available online 11 June 2020

Keywords:
CFD
Agglomeration
Collision
Discrete phase modeling
Spray drying
Eulerian-Lagrangian

ABSTRACT

Controlled agglomeration during spray drying offers several advantages for both powder manufacturers and consumers, and thus it is commonly implemented by industry. The implementation, however is largely based on experience, given the scarcity of comprehensive prediction tools. A resource-efficient approach to numerically treat agglomerates and yet provide an indication of their structures is desired to perform realistic simulations without the need for high-performance computing. In this work, a new numerical model for the treatment of coalescence and agglomeration was implemented and evaluated at two distinct scales with significantly different particle number densities within a Eulerian-Lagrangian CFD framework. The model could accurately predict the trends in the final particle size distributions and distinguish realistic agglomerate structures occurring under different conditions. Challenges were encountered as a result of how the underlying collision detection routine handles high particle number density. Several strategies are proposed to overcome these challenges. This work constitutes significant progress towards achieving an efficient prediction tool to estimate final powder properties and will prove useful in performing large-scale simulations to design and control agglomeration.

1. Introduction

Spray drying is a ubiquitous technique for efficiently producing high quality powder products in various industries such as the dairy, instant food, detergents, pharmaceuticals and agrochemicals industries. In spray drying chambers, the feed is converted into micro-sized droplets via atomization, which facilitates a favorable heat and mass transfer. The volatile component from the sprayed droplets is extracted by the drying medium resulting in final powder products. Producing this powder with a well-controlled particle size distribution (PSD) as well as particle shape and structure is of paramount interest to industry. While the initial size distribution of the atomized droplets is one of the principal governing factors in determining the final size and shape of the particles in the powder product, numerous other factors such as the entire history of temperature, moisture content, physical properties as well as trajectory variables such as velocity and contact angle of the particles play equally important roles. The atomized droplets inevitably collide with each other, which leads to a continuous evolution of the particle size and structure. Alongside the breakage of primary droplets, there are three collision outcomes that cause significant change in the final particle size and structure, namely post-collision stretching and reflexive separation (leading to smaller satellite droplets); coalescence (collision partners completely merge or fuse together typically leading to a larger spherical droplet); and agglomeration (collision partners partially penetrate each other and form a new particle with sustained morphological changes).

It is well established that agglomeration significantly contributes to improving the rehydration and flow properties as well as reducing dust by binding the fine fractions, particularly when the wetting step is limiting [1–4]. Therefore, the current practice in commercial spray dryers, particularly in the dairy industry, is to employ forced secondary agglomeration for example by returning the fines near the atomizers [5,6]. Regardless of the specific method of inducing agglomeration,

Abbreviation: CDC, Characteristic Drying Curve; CFD, Computational Fluid Dynamics; DEM, Discrete Element Method (DEM); DPM, Discrete Phase Model; DSMC, Direct Simulation Monte Carlo; MP-PIC, Multiphase Particle in Cell; NTC, No Time Counter (NTC); PSD, Particle Size Distribution; SEM, Scanning Electron Microscope; SST, Shear Stress Transport; UDF, User Defined Function.

* Corresponding author at: Department of Chemical and Materials Engineering, The University of Auckland, New Zealand.
E-mail address: wai.woo@auckland.ac.nz (M.W. Woo).

https://doi.org/10.1016/j.powtec.2020.05.111
0032-5910/

achieving a controlled agglomeration that results in a defined PSD and desired bulk properties of the final powder remains a challenging task. The challenge is mainly caused by interactions between, and the combined effect of a number of process variables (shown in [5,7]). Moreover, the difficulties faced in achieving a fully optimized operation, which involves controlled agglomeration are amplified by the limitation that design, scale-up of spray dryers as well as determining suitable operating conditions thereof largely rely upon simple empirical models or a trial-and-error approach [8–10]. In contrast to the resource intensive experimental approach, an accurate predictive model of spray drying has the potential to improve product quality and develop novel processes as well as to reduce the trial costs [11].

In dealing with the challenges and acquiring a better understanding of such complex multiphase industrial processes, computational fluid dynamics (CFD) has proved extremely useful, owing to rapid advances in the CFD field and the availability of ever-increasing computational power at reasonable cost. Because of the flexibility and effectiveness of the technique, it has been applied since the 1980s in designing and scaling-up of spray dryers [12]. Since then, many researchers have justifiably employed CFD to model and investigate comprehensively various aspects of spray drying, including modeling the outcomes of inter particle collision [5,6,13–16].

The modeling of spray drying processes in the Eulerian-Lagrangian framework can either be performed in a transient simulation by simultaneously tracking all particles within the simulation domain, or in a steady-state simulation by employing a sequential tracking of particles. Particularly for collision modeling, the transient approach can be extremely resource intensive, in contrast to the steady-state approach which has the unavoidable disadvantage of neglecting the possible transient and dynamic nature of the flow patterns found to be present in virtually all spray dryers [17]. Regardless of the choice of the transient or steady-state solver, the modeling of agglomeration within the CFD-framework consists of three main consequential steps: (1) the search for potential collision partners; (2) the prediction of collision outcomes such as successful agglomeration, coalescence or separation; and finally (3) the numerical treatment of the resulting particles including the agglomerates.

Two approaches are usually employed in collision modeling, namely the stochastic approach and the deterministic approach. Pilot or large-scale spray drying simulations reported so far typically utilized the stochastic approach for collision detection, rather than the deterministic approach [18–20] that was identified to be numerically more expensive [14]. The algorithm for the standard stochastic approach to modeling collision phenomenon in a spray is based on the Direct Simulation Monte Carlo (DSMC) method first proposed by Bird [37], which was subsequently adapted to handle the phenomenon of an evaporating spray by O'Rourke [21]. The collision probability, in this approach, is calculated based on the kinetic theory of gases. In order to minimize the number of particle parcels (where a parcel is defined as one computational particle representing a collection of particles that are assumed to have the same properties throughout the flow field [22]) required in the CFD simulations, the calculation algorithm is based on the assumption that a collision between two parcels can only take place if they are located in the same computational cell. There are other variants of the abovementioned stochastic approach reported in the literature in which the statistical sampling is undertaken based on a fixed volume surrounding the particle irrespective of the volume of the discretized cell in which the Lagrangian particle is located [6]. This sampling approach was introduced to avoid the potential mesh dependence of the statistical framework [23–25].

After the detection of the potential collision partners, the next step is to determine whether or not these potential collision partners will in fact experience collision. The simplistic collision criterion proposed by O'Rourke [21], for the collision of liquid droplets without any dissolved solids, first determines if the potential collision partners will just graze each other (leading to unsuccessful collision) or coalesce. Subsequently, the fates of the collision are determined by comparing the distance of the contributor from the collector droplet center with a calculated critical offset. In a modified version [6] of the O'Rourke model, the same collision outcomes were determined by the angle of impact.

In a series of reports from the group of researchers led by Sommerfeld, the concept of a collision efficiency in determining the collision outcome of the statistically characterized potential collision particles was reported. The collision model of Sommerfeld [26] was extended by Ho and Sommerfeld [15] by accounting for the collision efficiency for different sized particles and introducing coalescence criteria founded on energy balance. In the sensitivity study conducted by applying the extended model, it was found that high particle concentration, stickiness and large size ratio between particle size classes favor the agglomeration process.

In another study, the critical moisture content of the particles was used as a criterion to distinguish between wet and dry particles, as well as to determine the efficiency of successful wet particle collision [13]. Moreover, an "agglomeration probability" was introduced to determine the likelihood of agglomeration, which directly determined the number of collisions that resulted in agglomeration. The phenomenon of dry particle agglomeration was captured in the same study [13] by employing the concept of van der Waals force adopted from the work of Ho and Sommerfeld [15].

Exploring alternative approaches revealed that another group of researchers implemented O'Rourke's model to account first for the droplet-droplet collision only [27] and later for particle-particle interactions [28] and they showed that the inclusion of collision phenomena markedly affected the temperature and humidity of the continuous phase. The temperature and humidity of the continuous phase were influenced, presumably because particles of different sizes and properties were calculated depending on the determined collision outcome, which altered the predicted heat and mass transfer between the two phases. The researchers combined the O'Rourke algorithm to detect the collision with the hard-sphere approach [29,30] – originally developed for the field of fluidized bed hydrodynamics and granular dynamics – to determine the interactions between particles. However, in the developed model, agglomeration was not considered. The drawback of such a hard-sphere approach is that it does not allow for penetration of particles as a possible outcome, which is crucial in modeling of agglomeration of wet and viscous particles.

Following the collision detection and outcomes, as mentioned earlier, the final step is the numerical treatment of the resulting particles. Regardless of the collision detection and collision outcome model used, all of the CFD simulation works discussed so far numerically treat the final coalesced and agglomerated droplets/particles as spherical while the total mass of the colliding particles is conserved. While this approach is suitable for coalesced droplets, using the same numerical treatment for the agglomerated particles means that important information on the structure of the agglomerate is inherently sacrificed. This information is of primary interest for understanding the agglomeration processes. However, preserving such information is not possible, as the different approaches described above either treat the prediction of collision outcomes as a 'cut-off' process or they manipulate the proportion of successful collisions, without calculating the degree of fusion or sticking of the wet particles. To the best of our knowledge, the only CFD modeling work for spray drying, which computes the degree of penetration or fusion between wet particles by considering the dissipation of the kinetic energy during the collision process is given in the EDECAD project [5], even though the penetration depth was not utilized further. This approach in the EDECAD project was described in more detail by Blei and Sommerfeld [31], who also implemented the updated the version of the model in CFD simulations performed for a pilot scale dryer. Even with such detailed information calculated as part of the collision outcome model, both abovementioned studies adopted the approach of simplifying with a spherical final equivalent particle. It is noteworthy that this model was further developed and utilized in several other studies involving agglomeration modeling [14,31–33].

One approach to overcome this limitation of treating the resulting agglomerate as an equivalent spherical particle is to model the collision dynamics and penetration of the colliding particles and then to store the position, inter-particle sticking force, and orientation of each primary particle forming the agglomerate in memory. This would enable the dynamic morphology of the agglomerate to be estimated. In a recent article, following the abovementioned approach, Sommerfeld and Stübing [14] extended the stochastic particle collision detection framework to model the collision and preserve the agglomerate structures. Referring to the assumption of using a volume equivalent diameter for the new agglomerate as a rather "crude" one, they suggested more appropriate alternatives such as the diameter of the equivalent convex hull, the gyration diameter, and the surface area equivalent diameter. In their energy balance-based approach, the newly formed agglomerates were still treated as point-particles in the Eulerian-Lagrangian framework; however, location vectors of the primary collision partners were stored and thus agglomerate structures were determined. Employing their model on a pilot-scale dryer [34] they reported promising results but only from some preliminary steady state simulations with 10,000 parcels. Satisfactory validation of the model could not be presented due to a lack of data and thus they highlighted the need for large-scale dryer simulation trials. Although their approach was claimed to be numerically efficient, all the simplifications and assumptions associated with the reported works indicate the prohibitive nature of the computational expenses that would be incurred by a transient large-scale spray drying simulation.

Therefore, there is a need for a novel approach that can numerically treat the agglomerate formed via the agglomeration process without inflating the computational requirements but can also provide an indication of the agglomerate structure delineated by the degree of penetration or fusion between the colliding particles. To achieve this, a new numerical scheme to be employed in Eulerian-Lagrangian framework was introduced in one of our previous works [35]. To maintain the inexpensive numerical requirement, the theoretical framework is still based on the use of the equivalent spherical agglomerate particle, but it incorporates the tracking of the 'reduced agglomerate surface area' at each particle collision to delineate the looseness or compactness of the agglomerate. In this way, the structure of the agglomerate could be indirectly described without the need for expensive tracking of individual primary particles that form the agglomerate. However, that framework had not been evaluated in a full CFD simulation of a spray drying process, and thus it was unclear if it was able to distinguish different agglomerate structures under actual agglomeration conditions (e.g. particle number density, or the degree of particle stickiness) encountered in a spray dryer.

In this work, we propose a new approach to modeling agglomeration during spray drying using CFD. In essence, we integrate the theoretically established idea [35] in the CFD simulation of spray drying in two scales of spray dryers: a lab-scale spray dryer (the basic setup of the CFD model as well as supporting experimental data were previously published in [36]) as well as a large-scale dryer (the basic setup of the CFD model and supporting experimental data were published partially in [37] and are supplemented by new trial data with fine returns). Experimental data were obtained from both spray dryers and were used to evaluate the overall performance of the model, gain further understanding and clearly identify the limitations associated with the proposed agglomerate structure preservation model. By means of the evaluation at both lab-scale and large-scale spray dryers, we also identified several important considerations in the implementation of the O'Rourke collision detection scheme which was used as the basis of the agglomeration model in this work.

On the mesh dependence of O'Rourke's collision detection routine

This work utilizes in core the O'Rourke collision algorithm due to its overwhelming advantages in contrast to the limitations. However, in order for the readers to better appreciate and interpret the findings, a brief account of the established limitations must be provided. To this end, a review of previous studies that attempted to overcome these limitations is provided here.

O'Rourke's collision algorithm, which was originally developed to deal with an evaporating spray in 1981 [21], is based on the DSMC method first developed and applied to a flow problem by Bird [38]. Further details including a comprehensive account of historical evolution of the method can be found elsewhere [39]. O'Rourke's algorithm very quickly became the standard approach to numerically simulating collisions in Lagrangian framework. Even though droplets being represented by parcels which enabled only a fraction of the real number of droplets to be calculated reduced the computational costs by several orders of magnitude, the method was still found to be prohibitive and hence a new method was proposed by Schmidt and Rutland [25] based on the No Time Counter (NTC) algorithm. This new method was reported to be able to reduce the required number of calculations that became linear with respect to the number of parcels, compared to the quadratic requirement of O'Rourke's model. Moreover, this method was reported to show comparatively less mesh dependence [40]. To reduce the mesh dependence even further, adaptive meshing was introduced later in this method by Hou and Schmidt [41], who also incorporated formation of satellite droplets due to stretching and reflexive separation in their model as possible collision outcomes. Such breakage of droplets induced by collision was reported to be one of the dominant phenomena in atomization processes, particularly with an inter-spray impingement systems and ignoring of this phenomena was suggested to be one of the major reasons behind the overprediction of coalescence and subsequent droplet size by O'Rourke model [42]. Addressing the remaining mesh dependence and other challenges such as momentum imbalance of the NTC method, Li, Cai, He and Hu [24] proposed an alternative method based on the smoothed particle hydrodynamics (SPH) principle and reported it to be more accurate, resource-efficient and mesh-independent. Zhang, Mi and Wang [23] also battled the mesh-dependence of O'Rourke model by employing an adaptation of the search volume for collision partners.

Deviating from the conventional Lagrangian calculations, Andrews and O'Rourke [43] developed a disparate method called Multiphase Particle in Cell (MP-PIC) for dense particulate flows while stating that the Lagrangian framework is unsuitable and unable to realistically resolve collision calculations for discrete phase volume fractions above 5%. Hence the particle collision frequency predicted by original O'Rourke's algorithm may be unrealistically high. Later to include the particle collision phenomena in the developed MP-PIC method, a series of works was published. The general calculation method was introduced in the first [44] of the series of papers, while the following two papers reported further improvements and extension of the model, such as inclusion of collision damping due to non-elastic collision [45] and incorporation of additional effect to drive the particle velocity distribution towards isotropy [46]. Despite all the developments (including but not limited to the abovementioned works) in the last four decades since the introduction of O'Rourke model, it still remains the most useful, widely applied and popular collision algorithm. It was regarded as the standard approach in Lagrangian spray modeling by many researchers [e.g. 23, 25, 42] and is until now the default approach used in many commercial CFD packages.

2. Material and methods

2.1. Experimental data, calculation domain and boundary conditions

The lab-scale experimental data were obtained from a previously published work [36]. All relevant details on system description, methods, and measurements are provided in detail in the cited work.

The large-scale dryer was also reported in detail in a previous work [37] including the experimental details. Hence the description is not repeated here. However, for the convenience of the readers, sketches of the experimental rigs are shown in Fig. 1. The major difference to the operation of the large-scale trials reported in the cited study [37] was that in the current study the fine returns in the atomizer region was employed through cooling air inlet 2. The mass flow rate of the fine fraction was measured by logging the feed rate over a 15-min interval. The average mass flow rate of the accompanying air used as a carrying medium for the fines was measured to be approximately 231.6 kg/h. The atomizer was equipped with a pressure nozzle (i.e. spray Dry SK-orifice insert index 72 (0.63 mm), core insert 21, hollow cone spray angle 55°) operating at 200 bar. Table 1 shows the operating conditions used in the investigated trials (for abbreviated points of measurements please refer to Fig. 1b). Following the trials, samples from both the static fluidized bed and the fine fraction were collected and investigated to determine the moisture content as well as the PSD. The moisture content of the powder was determined by the weight loss recorded after drying 2 g of the powder sample mixed with sand in an oven at 105 °C for 7 h. At least two samples were analyzed for each case. Bulk density of the powder samples was obtained by weighing a measuring cylinder filled with powder, and tapped density was obtained by recording the sample volume after tapping the same filled cylinder used for measuring the bulk density for 180 times. The PSD was measured by laser diffraction in a Malvern Mastersizer 3000 (Malvern Instruments Ltd., UK) device. During the PSD measurements a dry cell was employed, where compressed air was used as the dispersion medium with a pressure fixed at 400 kPa and the sample was fed with a vibration fixed at 30%.

Another substantial difference to the already reported trials was the sprayed material. For this work in all large-scale trials, instead of whole milk, 40%wt skim milk reconstituted from commercial skim milk powder (Lactalis, France) at 45 °C was used as feed. Due to this change in trials, the droplet drying model was adapted as well. In order to accurately capture the drying kinetics of skim milk, complying with the previously validated simulation works, again the Characteristic Drying Curve (CDC) approach [47,48] was employed with the critical moisture content set to the initial solid content of 40%. The kinetics data as well as necessary correlations are available in the literature [48,49].

The primary atomization and the fine returns were modelled as a hollow cone and a group injection, respectively (see Fig. 2). Both injection types are inbuilt injection models available in the commercial package used [50]. The injection parameters are listed in Table 2. The origin of the hollow cone injection was chosen to be at the tip of the nozzle

Table 1
Conditions for the experimental trials and the dryer outlet and product characteristics.

Parameters	Run 1	Run 2
Spray rate, kg/h	202	210.5
Inlet air humidity, g/kg dry air (H1)(H4)	1.4	1.4
Primary hot air inlet flow rate, kg/h (F1)	2221.72	2732.5
Inner hot air annulus flow rate, kg/h	1662.5	2044.7
Outer hot air annulus flow rate, kg/h	559.2	687.8
Primary inlet air temperature, °C (T1)	224.6	175
Cooling air flow rate, kg/h (F2)	286	304
Cooling air 1 flow rate, kg/h	50.9	54.1
Cooling air 2 flow rate, kg/h	231.6	231.6
Cooling air 3 flow rate, kg/h	145.8	155.0
Cooling air 4 flow rate, kg/h	89.3	94.9
Cooling air temperature, °C	32.5	33.8
Fine returns (kg/h)	89.4	90.72
Static bed air flow rate, kg/h (F4)	660	648
Static bed air temp., °C (T4)	72.1	71.9
Outlet pressure, Pa gauge (P3)	−637	−490

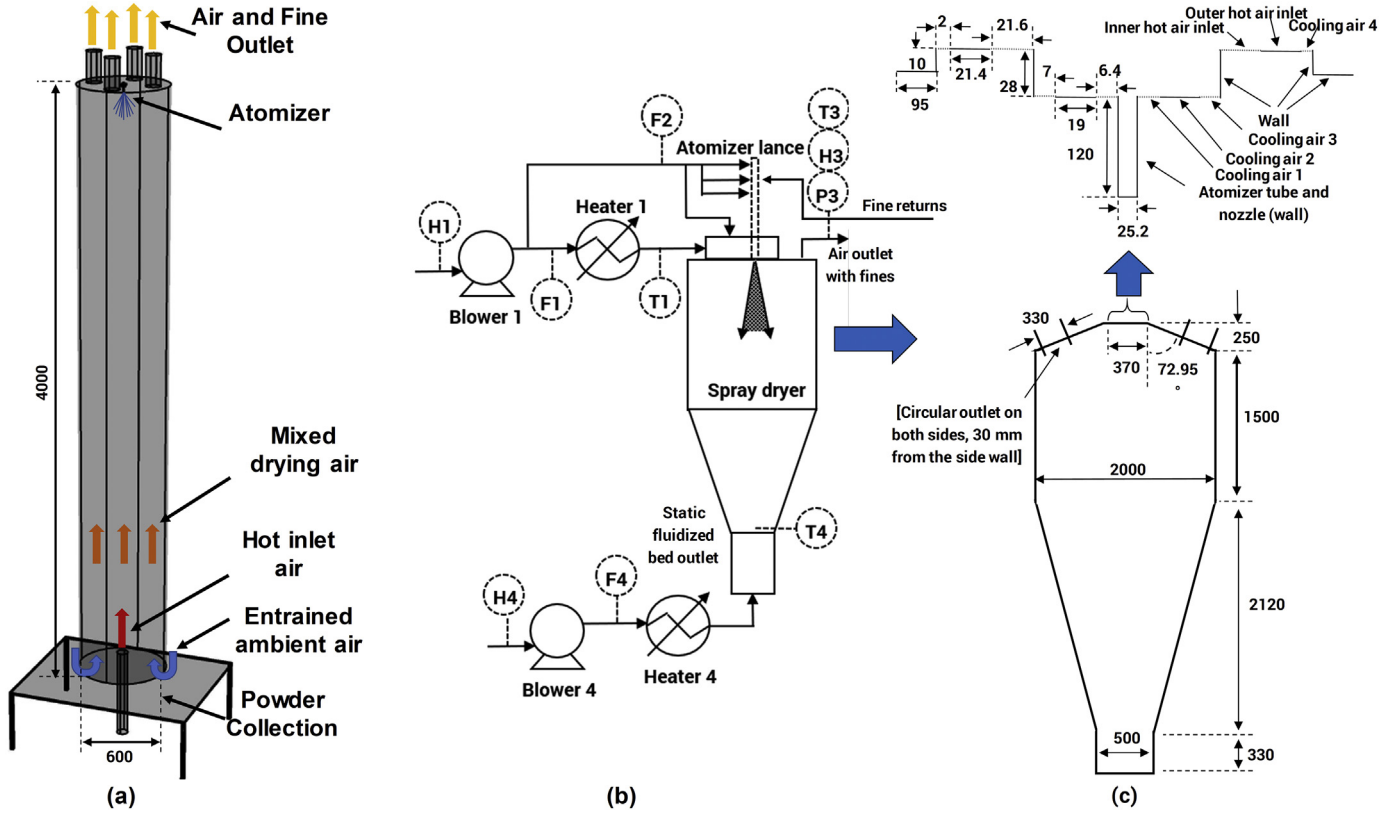

Fig. 1. Simplified schematic of the spray towers used in this study; (a) Lab-scale counter-current spray dryer, (b) arrangement of the large-scale spray drying chamber with all relevant point of measurements excluding the cyclones, (c) sketch of the large-scale spray drying chamber with all relevant dimensions (below) and the detailed configuration of the air inlets near the atomizer lance (above). (Drawings are not in scale; however, all provided dimensions are accurate and shown in millimetre. Illustrations were adapted from [36,37]).

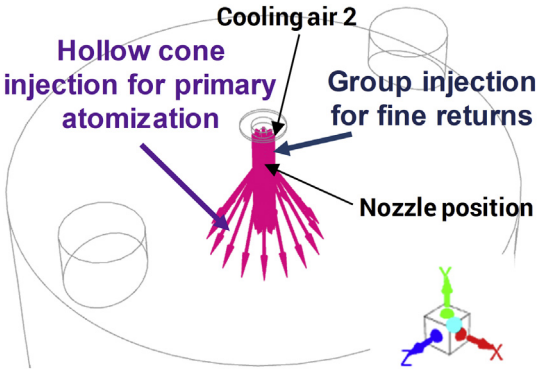

Fig. 2. Top section of the large-scale spray drying chamber (computational domain) showing the arrangement of the primary atomization (hollow cone) and the introduction of the fine returns (group injection through the inlet cooling air 2).

orifice with an outer radius of 0.3 mm. The swirl fraction of the hollow cone injection was set to zero. On the other hand, for modeling the fine returns, the group injection was used which was distributed along the annulus ring of the cooling air inlet 2. In order to have the fine returns distributed homogenously across the inlet, in total eight group injections equidistantly distributed along the perimeter were employed. Each of those group injections consisted of five streams, spreading from the inner radius to the outer radius of the annulus ring type inlet. Thus 40 parcels were injected per time step.

As already mentioned, different operating conditions were used for these two large-scale trials, specifically with fine returns, higher feed rate and a disparate feed material. In order to evaluate the accuracy of the predictions, the measured outlet temperature and moisture content were again compared with the predicted values. This comparison was used to support the previously reported validation with further evidence and the comparison can be found in Table 3.

2.2. Model description

The theoretical background as well as other relevant details pertaining to the modeling of drying kinetics, heat and mass transfer as well as particle motion are provided elsewhere [37] and therefore not repeated here due to brevity (Excerpts from the cited work are provided in the supplementary information for readers' convenience). Considering the focus of this work i.e. inter-particle collision and the outcome thereof, modeling details only pertaining to these phenomena or submodels are described in the following Sections 2.2.1 through 2.2.4. An overview of the calculation algorithm showing how the calculations are performed in a Eulerian-Lagrangian scheme is presented in Fig. 3a. The algorithm highlights the position of the collision routine, which might prove useful in better appreciating the following details provided in regards to the collision model. Fig. 3b then illustrates specifically the outline of the implemented collision algorithm.

Table 2
The parameters used in large-scale simulations to model the atomization and the fine returns.

Injection parameters	Primary atomization	Fine returns
Diameter range (μm)	5–200	5–150
Rosin-Rammler Mean (μm)	80.08	46.32
Spread Parameter (−)	1.9	1.97
Number of parcels (−)	200	40
Injection type	Hollow-cone with a full cone angle of 55°	Group injection comprising 8 points

Table 3
Comparison of CFD prediction of outlet conditions with measured values.

Quantity	Run 1	Run 2	Source
Outlet humidity, g/kg dry air (H3)	36.9	32.7	Measured
	37 ± 2	30.5 ± 1.6	Simulation
Outlet temp., °C (T3)	83.75	73.1	Measured
	83 ± 4.7	70 ± 3	Simulation
Product moisture content, %wt	4.87	6.25	Measured
	5.25	8.92	Simulation (above fluidized bed)
	1.96	2.12	Simulation (powder exiting all outlets combined)

2.2.1. Implemented variant of O'Rourke Collision Model

In lieu of assessing the geometrical information to determine whether or not a particle pair intersects in their path, the collision model developed by O'Rourke [21] employs stochastic method to estimate the collision phenomenon. This is why the model proved resource efficient. In the stochastic method, it is assumed that two particles may only collide if they are located within a certain volume, which is defined as the volume of the continuous phase cell. The model determines the collision probability from the perspective of the larger particle, which is defined as the collector and referred to in the following with the index of 1. On the other hand, the other collision partner with a smaller diameter is defined as the contributor and denoted below with the index of 2. The calculations take place in the frame of reference of the collector, which implies that the velocity v_1 is zero. Furthermore, this model implements the concepts of discrete parcel method [22], which means instead of tracking each particle, a parcel is tracked. A parcel is a statistical representation of a number of particles that are assumed to have identical properties as well as fates, which effectively reduces the computational costs. Therefore, the collector parcel and the contributor parcel considered in the collision algorithm consist of n_1 and n_2 individual particles respectively.

In O'Rourke's model, the particles within a parcel are assumed to be evenly distributed within the volume of the computational cell, where the parcel is currently located. In order for the collision to occur, the center of the particles of diameters d_1 and d_2 must pass within the distance of $(d_1 + d_2)/2$. Based on this premise, an area of a disk perpendicular to the trajectory of the contributor, which covers all possible positions for the contributor possibly leading to a collision, can be calculated. This area is that of a flat circle with the center coinciding with the collector:

$$A_{col} = \frac{\pi}{4}(d_1 + d_2)^2 \tag{1}$$

This area then leads to the collision volume:

$$V_{col} = \frac{\pi}{4}(d_1 + d_2)^2 v_{rel}\Delta t \tag{2}$$

where v_{rel} is the relative velocity and Δt is the duration of the time step used to integrate the particle trajectories. Now instead of checking whether or not the contributor parcel is currently located within the collision volume, the algorithm determines the probability of the contributor being located within the collision volume:

$$P = \frac{V_{col}}{V_{cell}} = \frac{\pi(d_1 + d_2)^2 v_{rel}\Delta t}{4V_{cell}} \tag{3}$$

Since parcels are being considered, the above equation must be modified to account for the number of particles in the parcels:

$$P = \frac{n_2\pi(d_1 + d_2)^2 v_{rel}\Delta t}{4V_{cell}} \tag{4}$$

The actual number of collisions is then estimated from the probability distribution, which, according to O'Rourke, follows a Poisson distribution given as follows:

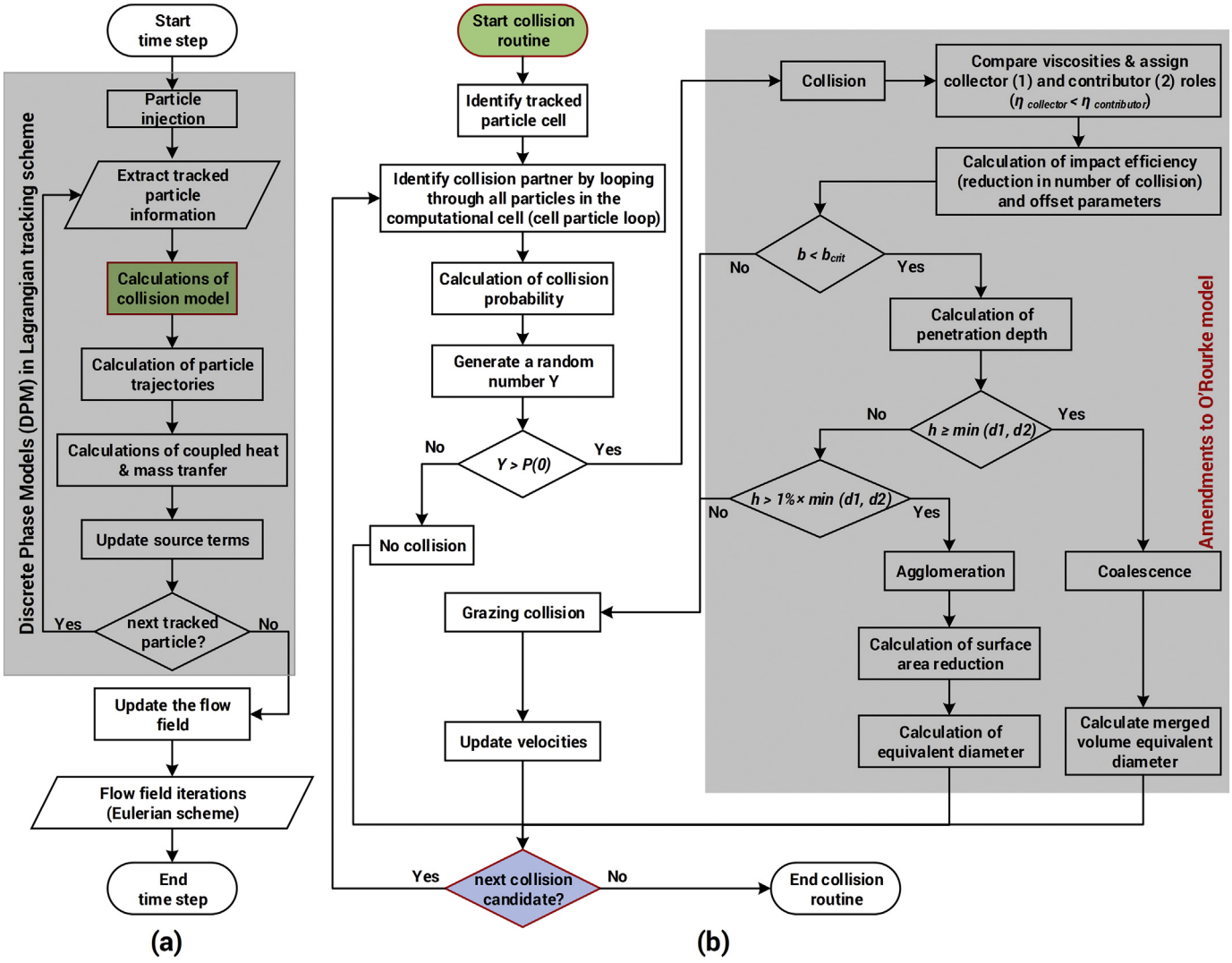

Fig. 3. Representation of the calculation algorithms in flow charts (a) overview of the calculation during each time step; (b) the collision routine consisting of the O'Rourke collision model alongside the suggested amendments used in this work (highlighted in the shaded rectangle).

$$P(N) = exp\{-\overline{N}\}\frac{\overline{N}^N}{N!} \tag{5}$$

where N represents the number of collisions for a collector with all other particles. Thus, in essence for each pair of tracked parcels located in the cell, the mean expected number of collisions is determined for each time step, and then finally a randomly generated sample from the Poisson distribution finally estimates whether this pair of parcels end up colliding into each other. Thus, the randomly generated number, Y is compared with the collision probability $P(0) = exp\{-\overline{N}\}$, and only if $Y > P(0)$, a collision is permitted.

In the case of a successful collision the algorithm estimates the outcome of the collision. Since O'Rourke developed the model for droplets, which cannot form agglomerate, only coalescence or grazing collision are considered as possible outcomes. The decision is taken based on the type of collision. It is assumed that an oblique collision would lead to a grazing collision, whereas a head-on collision will result in a coalescence. Therefore, the coalescence probability is related to the offset of the trajectory of the contributor with respect to the collector center as a function of the so called "collisional Weber number":

$$We_{col} = \frac{\rho v_{rel}{}^2 (d_1 + d_2)}{2\sigma} \tag{6}$$

where ρ and σ are the density and surface tension of the collector respectively, and v_{rel} is the relative velocity of the two parcels. O'Rouke suggested the following expression to calculate the critical offset parameter:

$$b_{cr} = \frac{(d_1 + d_2)}{2}\sqrt{\min\left(1.0, \frac{2.4f}{We_{col}}\right)} \tag{7}$$

where f is a function of the diameter ratio d_1/d_2 and is defined as:

$$f\left(\frac{d_1}{d_2}\right) = \left(\frac{d_1}{d_2}\right)^3 - 2.4\left(\frac{d_1}{d_2}\right)^2 + 2.7\left(\frac{d_1}{d_2}\right) \tag{8}$$

The actual collision parameter is calculated using a random number Y lying between 0 and 1 according to the following expression:

$$b = \frac{(d_1 + d_2)}{2}\sqrt{Y} \tag{9}$$

In the case of $b < b_{cr}$, the collision outcome is assumed to be coalescence. Otherwise, a grazing collision is predicted. For grazing collisions, the new velocities are determined based on the conservation of momentum and energy, where some fraction of the kinetic energy is assumed to be lost due to viscous dissipation and conversion into angular momentum. Again, the offset parameters are used in the correlation:

$$v_1' = \frac{m_1 v_1 + m_2 v_2 + m_2 (v_1 - v_2)}{m_1 + m_2} \left(\frac{b - b_{cr}}{\frac{d_1 + d_2}{2} - b_{cr}} \right) \tag{10}$$

$$v_2' = \frac{m_1 v_1 + m_2 v_2 + m_1 (v_2 - v_1)}{m_1 + m_2} \left(\frac{b - b_{cr}}{\frac{d_1 + d_2}{2} - b_{cr}} \right) \tag{11}$$

The proposed collision routine is based on the collision model developed by O'Rourke (described above). The modifications are made after the point when a collision is detected (shown in Fig. 3b under the dark shade). In other words, our proposed model finds a collision partner and estimates the mean number of collisions, following the identical steps as in O'Rourke algorithm. However once two collision partners are identified, the collector and contributor roles are assigned based on the viscosity, in contrast to the diameter size comparison in the original routine. This decision criterion was amended based on the considerations required for physical agglomeration phenomenon, where the size of particles is less relevant than their dynamic viscosity. In the model proposed in this work, it was assumed that the particle with higher viscosity (contributor) will penetrate that with lower viscosity (collector). Nevertheless, it must be noted here that the inherent prerequisite of the calculation of the critical offset parameter (Eqs. (7) and (8)) assumes that d_1 is larger than d_2. Owing to this assumption, it was ensured that the ratio d_1/d_2 is always calculated from the ratio of the larger diameter to the smaller diameter regardless of their roles in the particular collision.

The second modification stems from the idea that not every detected collision at this point would lead to a definite outcome. In the literature, this effect is defined as “impact efficiency” and according to Pinsky, Khain and Shapiro [51] the influence of this collision efficiency is more pronounced for markedly heterogenous sizes of the collision partners due to their aerodynamic interactions. The following mathematical description of this efficiency as a function of the relative Stokes number St_{rel} was suggested by Schuch and Löffler [52], and has been employed by other researchers [e.g. 5, 14] in collision modeling:

$$\eta_{col} = \left(\frac{St_{rel}}{St_{rel} + a_1} \right)^{a_2} \tag{12}$$

$$\text{with } St_{rel} = \frac{\rho_2 \, v_{rel} \, d_2^2}{18 \, \mu \, d_1} \tag{13}$$

The values of the constants a_1 and a_2 are dependent on collector particle Reynolds number:

$$Re_1 = \frac{\rho \, v_{rel} \, d_1}{\mu} \tag{14}$$

The constant values for various ranges were presented in a table by Sommerfeld and Stübing [14], who also aptly summarized the correlation between the impact efficiency and the dimensionless numbers. With increasing St_{rel}, which indicates that the response time of the contributor is high with respect to the available time to pass the collector, the impact efficiency rapidly grows. An increase in collector Reynolds number also leads to larger impact efficiency. This impact efficiency was used to determine the maximum lateral distance between the collision partners which would allow the occurrence of a collision. In the original O'Rourke algorithm however, the lateral distance is not used to decide for a collision, which is why the impact efficiency was used in our implementation to reduce the collision frequency, which indirectly accounts for the blocking effect discussed by Sommerfeld and Stübing [14].

The main difference between the current and the original O'Rourke framework starts in the implemented framework after the critical offset parameters are calculated using the Eqs. (7) through (9). For cases of oblique collisions i.e. $b < b_{cr}$, grazing collision is decided and new velocities are calculated. Unlike in the original O'Rourke collision routine, which only allowed for coalescence or grazing collision, a criterion for a third outcome i.e. agglomeration had to be incorporated. In order to achieve this distinction, the penetration depth has to be calculated first (described in Section 2.2.2). If the depth was found be equal to or more than the smaller of the participating parcel diameters, a complete coalescence was decided. In this case a volume equivalent diameter is calculated:

$$d_{p,coalesced} = \sqrt[3]{\frac{6(V_1 + NV_2)}{\pi}} \tag{15}$$

In order to hinder the occurrence of the agglomerates, that may become unstable due to very little penetration and thus be susceptible to breakage even on any insignificant impact, a minimum limit for penetration depth was defined to be 1% of the minimum of the participating dimeter sizes. This limit was assigned arbitrarily due to lack of experimental data, and aims to allow for the consideration in principle. The actual limitation modeling can be further honed by experimental data of agglomerate stability when available. At any rate, if an agglomerate is deemed not sustainable, a grazing collision is taken as the ultimate outcome.

Furthermore, the collision routines are proposed to be bypassed during the first 0.1 s flow time immediately after the injection, in order to allow for dispersion of the particles to progress prior to any coalescence. Since the collision routine loops through all particles residing in a cell, if collision is allowed prior to dispersion, it may lead to marked overprediction of coalescence, especially for the small time step size used in the simulation. Surprisingly, this strategy has never been reported before in past reports. It is envisaged that for future simulation work, the choice of the initial dispersion time should depend on the initial injection velocity and other injection parameters. It must also be noted that the dispersion lag per definition should be measured and decided in time and not in the number of time steps. In this work, the dispersion lag was chosen to be 0.1 s which was realized through 2 initial fluid-flow times steps, as the fluid-flow time step size was 0.05 s.

Now if the calculated penetration depth falls between the defined maximum and minimum limit, the outcome is assumed to be a successful agglomeration. In that case, the new equivalent diameter is calculated, which is further used for other calculations performed in remaining submodels such as heat and mass transfer, trajectory via drag calculations, collision calculations in subsequent time steps. The calculation of the equivalent diameter employs a blending model of two different approaches, namely the volume equivalent and surface area equivalent diameter [35].

Once the diameter of the collector parcel and the number of droplets in the contributor parcel are updated, the agglomerate surface area and the maximum possible surface area are calculated, in order to determine the reduction in surface area and store as additional information for each newly formed agglomerate. By following this approach, even though an equivalent diameter is being calculated and used in other submodels, each particle is carrying additional information which provides more insight into the agglomerate properties and hence enables final powder properties to be more accurately predicted.

2.2.2. Calculation of the penetration depth and surface area reduction

Let us consider two particles participating in a collision, in which particle 1 has a lower viscosity than particle 2. In this scenario, it can be assumed for simplification that particle 2 is penetrating into particle 1. A simplified sketch is shown in Fig. 4:

Applying the Pythagoras theorem on the half of the intersection length, *a can be calculated as follows:*

$$a = \sqrt{\left(\frac{d_1}{2}\right)^2 - \left(\frac{d_1}{2} - h_1\right)^2} = \sqrt{\left(\frac{d_1}{2}\right)^2 - \left(\frac{d_1}{2}\right)^2 + 2\frac{d_1}{2}h_1 - h_1^2} = \sqrt{d_1 h_1 - h_1^2} \tag{16}$$

or also expressed in terms of the diameter of the contributor as follows:

$$a = \sqrt{\left(\frac{d_2}{2}\right)^2 - \left(\frac{d_2}{2} - h_2\right)^2} = \sqrt{\left(\frac{d_2}{2}\right)^2 - \left(\frac{d_2}{2}\right)^2 + d_2 h_2 - h_2^2} = \sqrt{d_2 h_2 - h_2^2} \tag{17}$$

Therefore, the following expression can be written:

$$d_2 h_2 - h_2^2 = d_1 h_1 - h_1^2 \tag{18}$$

Now plugging in the value of $h_2 = h - h_1$ and rearranging in terms of h_1 yields:

$$h_1 = \frac{h^2 - d_2 h}{(2h - d_1 - d_2)} \tag{19}$$

Analogously, h_2 can be expressed as:

$$h_2 = \frac{h^2 - d_1 h}{(2h - d_1 - d_2)} \tag{20}$$

The equivalent diameter of the contact area to be used in Stokes' law, which was developed for a full spherical particle, can be estimated by:

$$d_{cont} = 2a = 2\sqrt{d_1 h_1 - h_1^2} \tag{21}$$

The contact area during the collision is variable and can be expressed as:

$$A_{cont} = \pi\left(d_1 h_1 - h_1^2\right) \tag{22}$$

The force resisting the droplet's movement into the particle with low viscosity μ can be calculated using Stokes' law for viscous force:

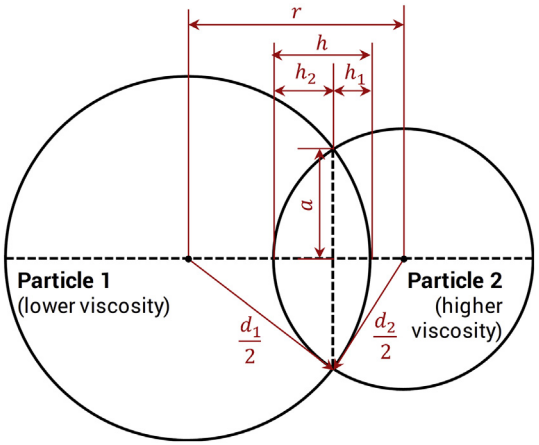

Fig. 4. Visualization of the penetration of particles in a head-on collision.

$$m_2 \frac{dv}{dt} = -3\pi\mu\, d_{cont} v \tag{23}$$

$$=> m_2 dv = -3\pi\mu\, d_{cont} \frac{dr}{dt}\, dt \tag{24}$$

$$=> m_2\, dv = -3\pi\mu\, d_{cont}\, dr \tag{25}$$

Substituting the value for contact diameter yields:

$$m_2\, dv = -6\pi\mu\sqrt{d_1 h_1 - h_1^2}\, dr \tag{26}$$

where, h_1 is a function of r. Therefore, h_1 must be expressed accordingly. We know that the total penetration, h can be expressed as:

$$h = h_1 + h_2 = \frac{d_1 + d_2}{2} - r \tag{27}$$

$$=> dh = -dr \tag{28}$$

Substituting the dr in the differential equation we have:

$$m_2\, dv = +6\pi\mu\sqrt{d_1 h_1 - h_1^2}\, dh \tag{29}$$

Replacing h_1 in $\sqrt{d_1 h_1 - h_1^2}$ with expression in terms of total penetration depth h followed by some simplification leads to:

$$\sqrt{h_1(d_1 - h_1)} = \frac{\sqrt{-h^4 + h^3(2d_1 + 2d_2) - h^2\left(d_1^2 + 3d_1 d_2 + d_2^2\right) + h\left(d_1^2 d_2 + d_1 d_2^2\right)}}{(2h - d_1 - d_2)} \tag{30}$$

Now integrating the differential equation from the initial conditions $v = v_0$ & $h = 0$ to the final condition $v = 0$ & $h = h_{max}$ leads to:

$$m_2 \int_{v_0}^{0} dv = +6\pi\mu \int_0^{h_{max}} \frac{\sqrt{-h^4 + h^3(2d_1 + 2d_2) - h^2\left(d_1^2 + 3d_1 d_2 + d_2^2\right) + h\left(d_1^2 d_2 + d_1 d_2^2\right)}}{(2h - d_1 - d_2)}\, dh \tag{31}$$

$$=> -m_2 v_0 = +6\pi\mu \int_0^{h_{max}} \frac{\sqrt{-h^4 + h^3(2d_1 + 2d_2) - h^2\left(d_1^2 + 3d_1 d_2 + d_2^2\right) + h\left(d_1^2 d_2 + d_1 d_2^2\right)}}{(2h - d_1 - d_2)}\, dh \tag{32}$$

The integral on the right-hand side of the above equation must be numerically determined, while the value of h is gradually increased and tracked until the integral value reaches $\frac{-m_2 v_0}{6\pi\mu}$. The final value of h will be the maximum penetration depth at which the contributor particle comes to a full stop. With this h, we can then calculate the surface area of the resulting agglomerate, which is the enclosed spherical segment area of both participants subtracted from the summation of the individual surface area:

$$A_{agg} = \pi\left(d_1^2 + d_2^2\right) - \pi(d_1 h_1 + d_2 h_2) \tag{33}$$

$$A_{agg} = \pi\left(d_1^2 + d_2^2\right) - \pi\left(d_1 \frac{h^2 - d_2 h}{2h - d_1 - d_2} + d_2 \frac{h^2 - d_1 h}{2h - d_1 - d_2}\right) \tag{34}$$

$$A_{agg} = \pi\left(d_1^2 + d_2^2\right) - \pi\left(\frac{d_1 h^2 - d_1 d_2 h + d_2 h^2 - d_2 d_1 h}{2h - d_1 - d_2}\right) \tag{35}$$

$$A_{agg} = \pi\left[\left(d_1^2 + d_2^2\right) - \frac{h^2(d_1+d_2) - 2d_1d_2h}{2h - d_1 - d_2}\right] \tag{36}$$

Finally, with the surface area of the agglomerate, the surface area equivalent diameter can be calculated for further tracking of the newly formed particle. However, on this note, it must be mentioned here that there is one critical limitation to the approach described above to determine the equivalent diameter. It was already shown elsewhere [35], that if only surface area equivalent approach is used, then beyond a certain penetration depth (i.e. a critical reduction in surface area) the calculated surface area equivalent diameter may become smaller than that of the volume equivalent sphere which stems from the concept of conservation of mass. A larger equivalent diameter than that of the volume equivalent sphere might justifiably imply that the effective density has decreased, enabling an inclusion of porosity of the agglomerate. By contrast, a smaller equivalent diameter would imply a compression of the particles, leading to an increase in the effective density and thus making it potentially even higher than the true particle density. The latter is obviously implausible. Therefore, in our model, a surface equivalent diameter is only allowed if it does not result in any compression. Otherwise, the volume equivalent diameter is used. The following expression mathematically describes the implementation of this strategy:

$$d_{p,agg} = \max\left(\sqrt[3]{\frac{6(V_1 + n_{col}V_2)}{\pi}}, \sqrt{\frac{A_{agg}}{\pi}}\right) \tag{37}$$

At any rate, the maximum possible surface area is the summation of the individual surface areas of the participating particles, which would occur if those participants barely touch each other:

$$A_{max} = \pi\left(d_1^2 + d_2^2\right) \tag{38}$$

The reduction in the resulting surface area, due to each agglomeration, is given by the ratio of the surface area of the agglomerate to that of the maximum possible surface area according to the following equation:

$$Z_{agg} = \frac{A_{agg}}{A_{max}} \tag{39}$$

The minimum surface area that an agglomerate can achieve is obviously the surface area of a completely coalesced particle as outcome, whereas the maximum limit of Z_{agg} is 1, when the collision partners barely touch each other and yet stick together. With the progression of further agglomerations of additional particles with the newly formed agglomerate, A_{max} and A_{agg} are further updated. As a result, A_{max} will keep becoming larger regardless of the penetration depth, whereas A_{agg} will strongly depend on the penetration depth h in each agglomeration. Subsequently, Z_{agg} will always keep becoming smaller and smaller. The calculation scheme is shown in Fig. 5. The compacter the agglomerates are or the more participants are involved, the smaller the final Z_{agg} will be. This will be a clear indication of the compactness of the agglomerates, without the need to preserve any information related to the shape, orientation and morphology.

There are two important considerations in calculation of the parameter of reduction in surface area. Firstly, the value of Z_{agg} can be updated, whenever a particle enlargement occurs, regardless of the collision outcome i.e. agglomeration or coalescence, which is causing the enlargement. In this way, the final Z_{agg} provides an overall indication of the agglomerate accounting for the impact of both types of particle collision outcomes on the resulting particle structure. Secondly by contrast, if we filter out all the incidents of coalescence and only update the Z_{agg} following a detected agglomeration, then this parameter could be utilized to interpret the structure of the agglomerates without the possible 'compact' region of the agglomerate stemming from potential coalescence instances. The Z_{agg} can then be visualized to provide an indication of the compactness or looseness of the porous part of the agglomerate structure i.e. the 'dendrites' of the agglomerate structure. With this activated filter, the higher the final value of Z_{agg}, the more occurrence of agglomerates consisting of loosely attached particles can be ascertained.

In other words, a higher Z_{agg} value would indicate that the agglomerate possesses more pronounced dendrites, whereas a lower Z_{agg} value would indicate that the structure is likely to be more compact showing less dendrites and a compact core. The abovementioned agglomerates are often referred to as "grape-structured", and "onion-structured" agglomerates respectively in the literature [53]. Regardless

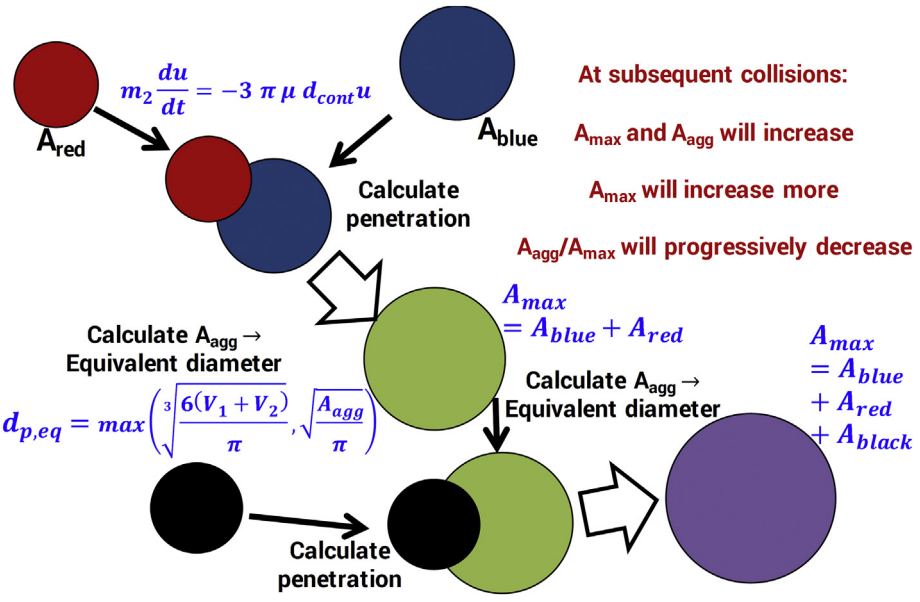

Fig. 5. Simplified visualization of the calculation scheme employed in the work to determine the equivalent diameter, and the reduction in surface area of an agglomerate (shown only for agglomerations, for coalescence the same scheme applies).

of whether the filter is activated or not, while the quantitative value of Z_{agg} provides a relative comparison, the overall magnitude of Z_{agg} can also provide an indication of the overall number of collisions that led to the resultant conglomerate. It must be noted here that with a large number of coalescence and agglomeration, which will become more apparent later in the results section, Z_{agg} can become extremely small in magnitude. We observed that for total number of collisions reaching over a million, depending on the size of detected collision partners, Z_{agg} can reach values in or around the order of magnitude of 10^{-10}. This is why, the plotted distribution curve might show fairly high fractions of size enlarged mass via coalescence and agglomeration corresponding to very low values of Z_{agg}.

2.2.3. Implementation of shrinkage for agglomerates

The shrinkage of droplets during drying was accounted for by employing the empirical linear shrinkage model [54]:

$$\frac{d}{d_0} = b + (1-b)\frac{X}{X_0} \tag{40}$$

The numerical implementation of shrinkage model in the CFD simulation is not described here for brevity, as it is provided elsewhere [55]. This subsection of the article was added to report about the difficulty in capturing the shrinkage behavior of the resulting particles arising from the collision outcomes. As can be seen from Eq. (40), the droplet shrinkage is estimated as a function of the ratio of the actual to initial moisture contents. Moreover, in this method, the initial diameter as well as the initial moisture content are crucial. However, following a successful collision outcome of coalescence or agglomeration, essentially a new particle is born. Considering the original initial diameter would now lead to an invalid actual diameter. Furthermore, by focusing on the physical phenomenon, if we consider the reason behind droplets deviating from the perfect shrinkage behavior, which is skin formation, we can safely assume that the skin is completely collapsed or at least partially disrupted by the penetration of the contributor in the collector particle. Now after this incident, how the shrinkage would actually progress, to the best of authors' knowledge, has never been studied. As a result, there is no model available in the literature to capture the post collision shrinkage behavior. The new development of such a model also falls outside the scope of this work.

Nevertheless, it would be also unacceptable to completely discard the shrinkage or continue with the pre-collision linear shrinkage. Therefore, as a method of estimation, we proposed that the particles following a collision are truly considered as newly born particles. This can be implemented in a way that after each collision, the progression of shrinkage for the resulting particle is reset. In other words, in terms of shrinkage calculation, the resulting particle is numerically treated as a newly born particle. Consequently, the calculated equivalent diameter and moisture content of the particle resulting from the collision are used as the initial parameters for further shrinkage estimation of that particle. These two additional pieces of information could be easily stored as user defined memory assigned to the particle. However, the other difficulty arises from the fact that the initial moisture content i.e. the moisture content of the newborn particle becomes variable, unlike that of the primary injected particles. As a result, the empirical shrinkage factor b can no longer be kept constant across the simulation. Fortunately, Fu, Woo, Selomulya and Chen [56] reported a linear correlation of the shrinkage factor as a function of the initial solid fraction $x_{solid,\,0}$ based on their extensive experimental data for skim milk:

$$b = 1.0287\, x_{solid,0} + 0.4387 \tag{41}$$

This correlation was employed to estimate the shrinkage factor for various particles. It is noteworthy that very few spray dried materials have such an extensive experimental database. For those materials lacking necessary experimental data to determine such correlation between the shrinkage factor and the initial solid content, the progression of the linear shrinkage behavior can be continued by calculating and storing a hypothetical initial diameter obtained from the resulting post-collision equivalent particle diameter, $d_{p,\,eq}$ as well as the moisture contents at atomization X_0 and at the time of collision i.e. that of the resulting particle $X_{p,\,eq}$:

$$d_{0,hypothetical} = \frac{d_{p,eq}}{\left[b + (1-b)\frac{X}{X_0}\right]} \tag{42}$$

This hypothetical initial diameter could then be utilized to estimate the degree of shrinkage until this particle undergoes any further coalescence or agglomeration.

2.2.4. Assumptions and limitations of the proposed model

While our agglomeration model aimed to improve on some areas, particularly to provide more accurate predictions of the collision outcomes, it still has the limitations of the original algorithm proposed by O'Rourke, that are given in [57]. The most important assumptions and limitations of our model are outlined in the following list:

- Frequency of collision is assumed to be considerably less than that of particle time step
- The model is suitable for low Weber number $We < 100$
- The model could display mesh-dependent artifacts
- Droplet break-up is not considered
- No elastic element is included in the calculation of the penetration depth
- No breakage of already agglomerated particles is incorporated
- Agglomeration of dry particles due to cohesive forces is not accounted for
- Wall deposition is not included and hence agglomerates formed by breakage of deposition is not considered
- The model implemented for impact efficiency was originally developed for smaller fine particles colliding with larger droplets
- The surface tension is not considered in calculation of penetration depth while determining the collision outcomes for simplicity
- The drag calculations assume the motion of a solid sphere in an infinite fluid for simplicity, even though the primary droplets/particles as well as the agglomerated/coalesced particles may be of various shapes

Further discussions intended by the authors as resources for future works that could address some of the abovementioned limitations can be found in Section 3.4.

Table 4
List and purpose of the user defined functions (UDF's) employed in this study.

Function designation	Purpose of the routine
`DEFINE_DPM_PROPERTY`	Specifying properties of discrete phase materials (such as density, viscosity, surface tension)
`DEFINE_DPM_TIMESTEP`	Limiting the time step size of the discrete phase model
`DEFINE_DPM_OUTPUT`	Modifying the output (data) of the written file associated with any sampling for postprocessing/analysis
`DEFINE_DPM_VP_EQUILIB`	Implementing the lump parameter model to account for appropriate drying kinetics
`DEFINE_DPM_SCALAR_UPDATE`	Updating scalar quantities (such as user defined particle memory) associated with particles
`DEFINE_DPM_SPRAY_COLLIDE`	Modifying the spray collision algorithm i.e. the algorithm for predicting collision occurrence (O'Rourke) as well as collision outcomes

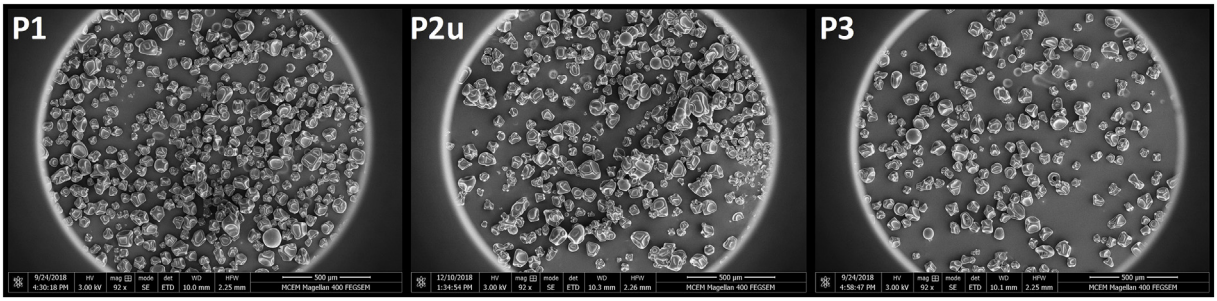

Fig. 6. Scanning electron micrographs of skim milk powder samples collected from the experimental trials conducted on the lab-scale dryer. Comparison of particle distributions of the representative samples are shown demonstrating the differences in agglomerated/coalesced particle structures among the discussed configurations, Pos 1 (left), Pos2u (middle) and Pos 3 (right).

2.3. Numerical solution and postprocessing

CFD simulations were performed by employing the pressure-based 3-D double precision solver in ANSYS Fluent (Release 2019 R3). All transport equations were discretized in second order upwind scheme, and the transient calculations were formulated in second order implicit scheme. Turbulence was modelled by utilizing $k-\omega$ SST turbulence model, for which detailed justification can be found in a previous publication by the authors [58]. "Enhanced wall treatment" was enabled for wall boundary conditions. The discrete phase (particles) was two-way turbulence coupled with the continuous phase, and was forced to reflect upon impact with the wall by activating the "reflecting" wall boundary condition with a coefficient of restitution of 1.

In order to determine the PSD and other average discrete phase properties such as moisture content, the numerical sampling in the CFD model at different boundaries was undertaken for 60 s for both spray dryers. The sampling time was initially chosen based on the average residence time of the particles (sampling duration was chosen to be at least double the average residence time) and finalized based on the observed stagnation in the change in the results with increasing duration.

A number of user-defined functions (UDF's) enabled the default package of ANSYS Fluent to be adjusted as well as additional or alternative (proposed) models to be incorporated. A list of all UDF's along with their respective purpose are given in Table 4.

The paragraphs above mention only key information about the simulation set-up. It must be noted here that both of the base models, i.e. lab scale and commercial scale, used in the CFD simulations were adequately validated with experimental data in previous studies [36,37]. Interested readers can refer to those articles for detailed description of the initial and boundary conditions implemented, the simulation set-up, property-data, grid-independence test, flow-field development and the implementation of user-defined functions.

The CFD simulations were performed using multiple desktop computers equipped with processors of base clock speed, ranging from 2.1 GHz to 3.4 GHz. Consistently for all simulations, 8 cores were utilized in parallel processing. The computers had at least 16 GB of memory installed. Roughly 48 h were required to complete a representative simulation (DPM time step: 10^{-4} s) of the lab scale dryer for a flow time of 120 s and that of the large-scale dryer for a flow time of 75 s. The average time to complete the calculations within a single time step was found to be heavily governed by the number of parcels as well as computational cells in the domain, and the time step size.

3. Results and discussion

3.1. Simulations of lab-scale counter-current spray drying

As reported in one of our previous works [36], trials were conducted on the lab-scale counter current spray dryer with various double nozzle

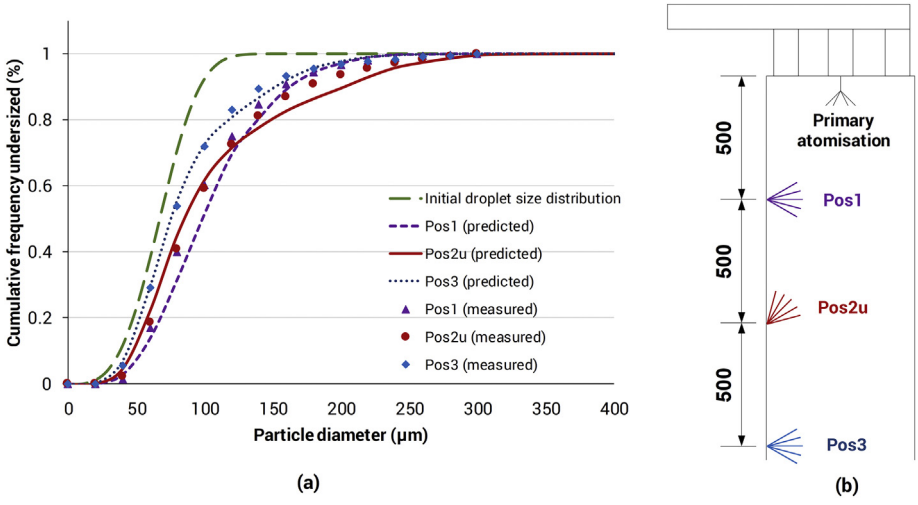

Fig. 7. (a) Comparison between the measured and predicted particle size distributions of the powder samples collected at the bottom outlet of the lab-scale counter current spray dryer for three different double nozzle configurations. (b) Schematic illustration of the top part of the dryer highlighting the differences among the tested double nozzle configurations (for further information refer to [36]). In addition to the differences in height of the secondary nozzle among the various configurations, for Pos2u it was positioned at a 45° upward angle, whereas Pos1 and Pos3 had horizontally placed secondary nozzles.

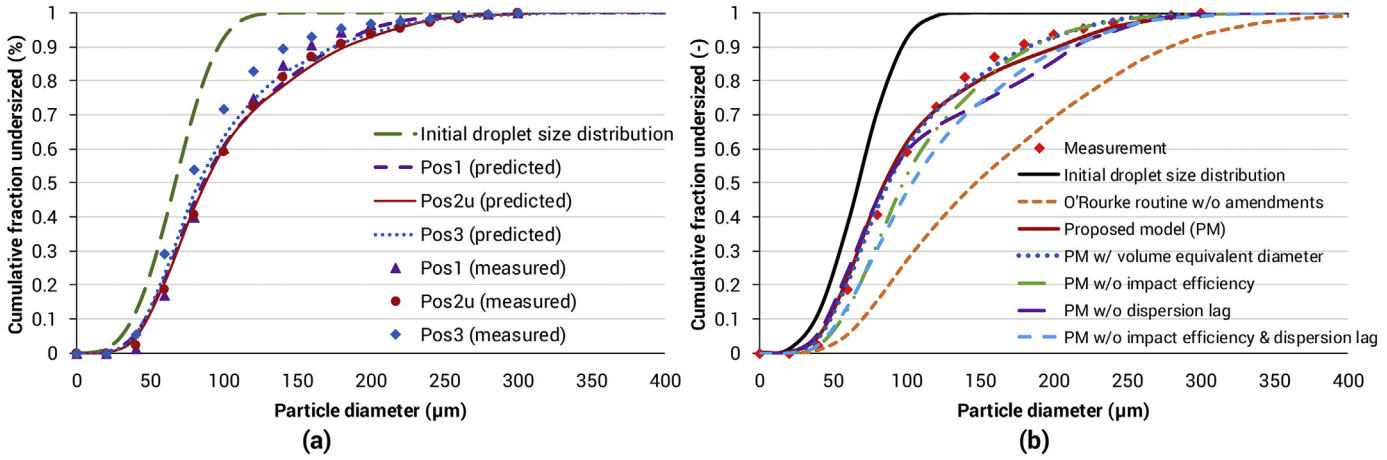

Fig. 8. (a) Demonstration of the effect of implementing volume equivalent diameter by comparing the measured and predicted particle size distributions of the powder samples collected at the bottom outlet of the lab-scale counter current spray dryer for three different double nozzle configurations. (b) The impact of implementing various approaches in modeling collision outcome on the final predicted particle size distribution of the product for the double nozzle configuration Pos2u in the tested lab-scale counter current spray dryer.

configurations. The PSDs of the collected powder samples were found to be significantly different in fractions found in different size classes. As a result, all representative diameters, such as sauter mean diameter ($d_{3,2}$) as well as diameter size intercepts for 10% (d_{10}), 50% (d_{50}) and 90% (d_{90}) cumulative mass, were also found to be different. This enabled the extents of size enlargements achieved via each configuration to be clearly identified. Among those trials of 6 different configurations, three configurations were chosen based on the observed differences in measured data for conducting CFD simulations with the proposed agglomeration model. For all configurations with the primary nozzle at the top, a secondary nozzle was employed to introduce a secondary atomization at different heights 500 mm, 1000 mm and 1500 mm away from the primary nozzle, which were labelled as Pos1, Pos2u and Pos3, respectively (as shown in a simplified sketch in Fig. 7b). For Pos2u, in addition to the distance from the primary nozzle, a 45° upward angle for the spray was introduced. It was established on the basis of the evidence of PSD data (as shown in Fig. 7a) as well as scanning electron microscope (SEM) images (as shown in Fig. 6) that Pos2u led to the highest particle size enlargement and most agglomerated particles, followed by Pos1 and Pos3.

CFD simulations were performed on all three double nozzle configurations. After the flow field was fully developed, particles were numerically sampled in the CFD models at both outlets (bottom powder collection and top air outlet) for 60 s. The particle samples were then analyzed to determine the PSD which is presented with the measured data in Fig. 7a. From the comparison, it can be seen that the predicted PSDs agree well within reasonable accuracy with the measured data. For both Pos1 and Pos3, the predictions closely match the experimental data, while for Pos2u a slight overprediction can be seen in the diameter-range 125–225 μm. The applied model could successfully predict the observed trend, even resolving the small differences among the runs. While all configurations led to some size enlargements as compared to the initial droplet size distribution, it was evident that Pos3 led to the smallest size enlargement across all size classes. Pos1 yielded higher size enlargements initially up to 125 μm particle size, beyond which for the rest of the size range 125–300 μm the size enlargement observed in the case of Pos2u was significantly higher. In Fig. 7a, it can be seen that this difference in size enlargements between Pos1 and Pos2u is reflected by the lower fractions of particles for the size classes below 100 μm for Pos1 as compared to Pos2u and the crossing of the both cumulative distribution curves at 125 μm. Moreover, beyond 125 μm it can be clearly seen that the size distribution for Pos2u stretches up to a significantly higher particle size, where 100% of the undersized particles is observed. These observations clearly indicate that Pos2u must have led to more agglomeration and coalescence, as compared to the other two positions.

In order to understand the contribution of different measures taken in the different approaches to modeling the agglomeration, the same simulation was performed with various approaches and the data were sampled and analyzed in an identical manner. One of the most critical differences between our proposed model and the conventional approach is the use of a novel approach involving surface area equivalent diameter instead of a purely volume equivalent diameter to determine the post-agglomeration particle size. Therefore, the simulation data for all configurations obtained via the volume equivalent approach are compared with the measured data in Fig. 8a, to clearly identify the effect on the final PSD. For Pos2u, the prediction obtained using the volume equivalent approach is even closer to the measured data than that obtained from the proposed model. In contrast, the discrepancies in predicting the PSD with the volume equivalent approach for Pos1 and Pos3 are fairly similar and markedly higher respectively. It is noteworthy that both approaches utilize a representative and numerical equivalent diameter in lieu of the actual diameter. Hence, exactly matching the predicted distribution with the experimental data should not be the main objective. The more significant accomplishment should be the ability to predict the proper trend and more importantly to resolve the differences among the various trials. From the comparison presented in Fig. 8a, it is evident that this important objective cannot be achieved with the volume equivalent approach.

Fig. 8b shows the effect of other approaches as well as individual measures implemented in the proposed model on the final PSD. For instance, the O'Rourke collision model, without any of the amendments shown in Fig. 3b in the shaded rectangle or described in Section 2.2.1, markedly overpredicts the size enlargement across all diameter classes.

The impact efficiency implemented in the proposed model appears to have affected the fractions below 150 μm more than the higher sized particles. This indicates that in the formation of relatively larger particles, the impact efficiency does not contribute much, as presumably the efficiency comes close to 100%. By contrast, the dispersion lag (allowing the first 0.1 s flow time for droplet dispersion before activating the collision routine), which has almost the opposite effect to the impact efficiency. With deactivated dispersion lag, a substantially higher fraction of large sized particles in the range of 200–250 μm was generated, followed by a sudden drop in frequency in the 100–150 μm range (leading to an unusual sudden increase in the fraction found for the diameter size class around 225 μm in the PSD). This indicates a weakness of the core model for the prediction of the occurrence of

Table 5
Comparison of yields as well as mass distributions of particle size enlargement (i.e. coalescence and agglomeration) predicted by the CFD model among the tested double nozzle configurations. Samples were numerically collected for 80 s flow time at the bottom outlet.

	Pos1	Pos2u	Pos3
Total yield (g)	1.06	1.88	1.38
Coalesced mass (%)	95.5	90.9	97.1
Agglomerated mass (%)	3.5	8.4	1.9

collision. It is noteworthy that the collision detection is very sensitive to the number density of particles. As the underlying routine for collision detection considers all parcels residing in the same cell as collision partners, it is not unexpected that immediately following the atomization, high collision frequency and subsequently high number of coalescences could be predicted when the droplets are in extremely close proximity.

This theory with regards to the effect of the dispersion lag on the prediction of collision outcomes was confirmed with comparing the percentage of coalesced mass in the final powder sample with and without dispersion lag. It was found that deactivating dispersion lag increased the percentage approximately from 91% to 96%. Moreover, when a particle becomes large at the initial phase, it takes longer to dry, which leaves it prone to further coalescence and agglomeration. As a result, the overall effect on the PSD is manifested as an increase in fraction among the higher size classes. It is noteworthy that without the lastly mentioned amendments i.e. the impact efficiency and dispersion lag, the prediction by the modified model for collision outcomes still agrees fairly well with the measured data. These amendments led to slight decrease in size enlargements and hence shifted the overall prediction towards smaller particle sizes and thereby facilitated the differences among various trials to be better reflected. It is noteworthy that the importance of the dispersion lag increases as the time step decreases. However, following an improvement of the underlying routine for collision detection, the idea of dispersion lag may become redundant.

The next part of the discussion delves into further simulation results extracted from the runs to understand how these might inform us about the degree of agglomeration or coalescence. During each collision, the collision outcome as well as other relevant information such as maximum possible surface area and reduction in surface area are stored in particle memory. These are utilized to gain further insight into the collision outcomes and their effect on the final powder samples.

First, we investigated the total product yields. During the trials, it was observed that while all double nozzle configurations led to significantly higher yield of powder samples as compared to the reference single nozzle run, the Pos2u led to the highest yield among all runs, followed by Pos3 and Pos1. Unfortunately, due to the limitations of the experimental set-up, the total yield could not be weighed and hence only qualitative observations were carried out. It was observed that roughly double the amount of feed was required to be spray dried for Pos1, in order to collect the same amount of sample as in the case of Pos2u. It was hypothesized upon analyzing the PSD and SEM images (examples of the representative images are shown in Fig. 6) that the higher yield for Pos2u occurred due to the greatest extent of agglomeration. Due to more agglomeration and coalescence, less fine fraction was produced, which exited the counter-current dryer through the top outlet, eventually leading to a higher yield of powder. Therefore, it can be said that, for the same feed rate in a counter-current dryer, higher yield is a clear indication of greater particle size enlargement, even though an examination of the yield alone cannot reveal, whether this particle enlargement stemmed from agglomeration or coalescence.

The experimental observations could corroborate the simulation results. In contrast to the qualitative experimental observation, it was possible to distinctively identify the powder mass that included agglomerates from the detailed CFD simulation results. The mass yield of the numerically collected powder sample at the outlet as well as the distribution of coalesced and agglomerated mass among different nozzle configurations are presented in Table 5. It can be seen that Pos2u, which led to the largest particle size also led to the largest yield. The yield of Pos2u was roughly 1.8 times and 1.4 times higher than that in Pos1 and Pos3 respectively. Similar relative differences in the collected sample amount for the identical amount of spray dried feed were experimentally observed as well. Since the feed rate was identical for all runs, the higher yield also suggests that Pos2u had the least amount of fines leaving through the top air outlet. Pos1 had the least mass collected at the bottom, which can be attributed to the fact that this configuration had the highest likelihood of fines from both atomizations leaving the dryer through the top outlet before undergoing any coalescence or agglomeration. In contrast, for Pos3, the fines ascending from the secondary atomization still had slightly higher chance to merge with wet particles stemming from the primary spray. By comparing the fraction of coalesced and agglomerated fractions of mass, it can be seen that, Pos2u led to not only a higher absolute agglomerated mass but also a larger fraction of agglomeration than any other configuration. With 8.4% for powder sample obtained from Pos2u, the fraction of agglomerated mass was approximately 2.4 and 4.5 times higher than those found for Pos1 and Pos3 respectively. For all runs, the

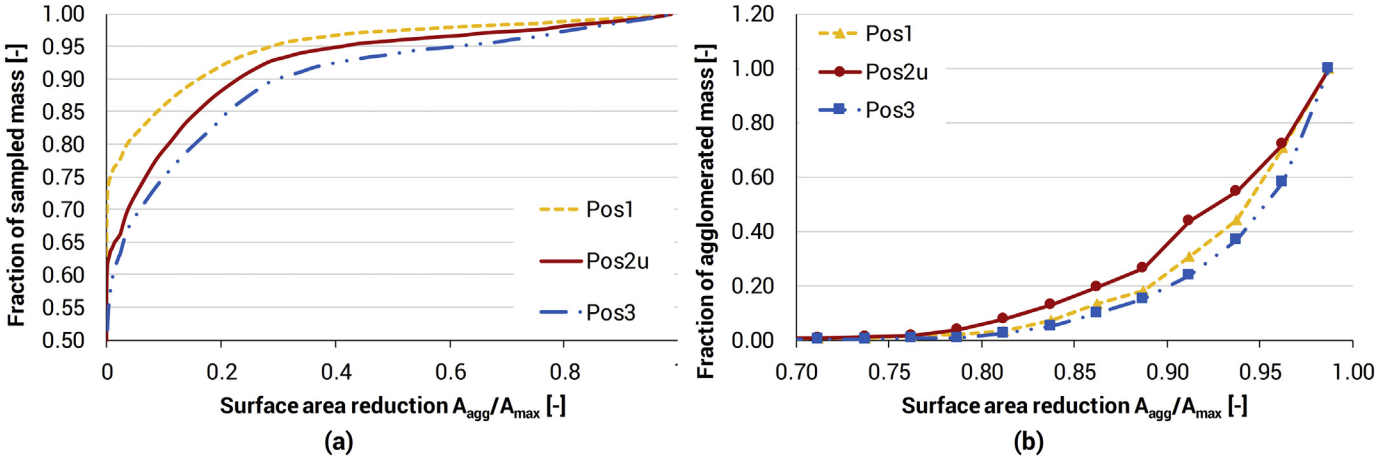

Fig. 9. Demonstrating the use of the surface area reduction to inform about compactness of the particles resulting from the runs with double nozzle configurations. The analyzed powder sample was collected during CFD simulations of all the tested runs of double nozzle configurations at the bottom outlet of the lab-scale counter-current spray dryer. (a) Comparison of the predicted distribution of the size enlarged mass as a function of the surface area reduction due to both coalescence and agglomeration. (b) Representation of the predicted cumulative distribution of the agglomerated mass as a function of the surface area reduction due to agglomeration only i.e. excluding coalescence demonstrating only the extent of agglomeration.

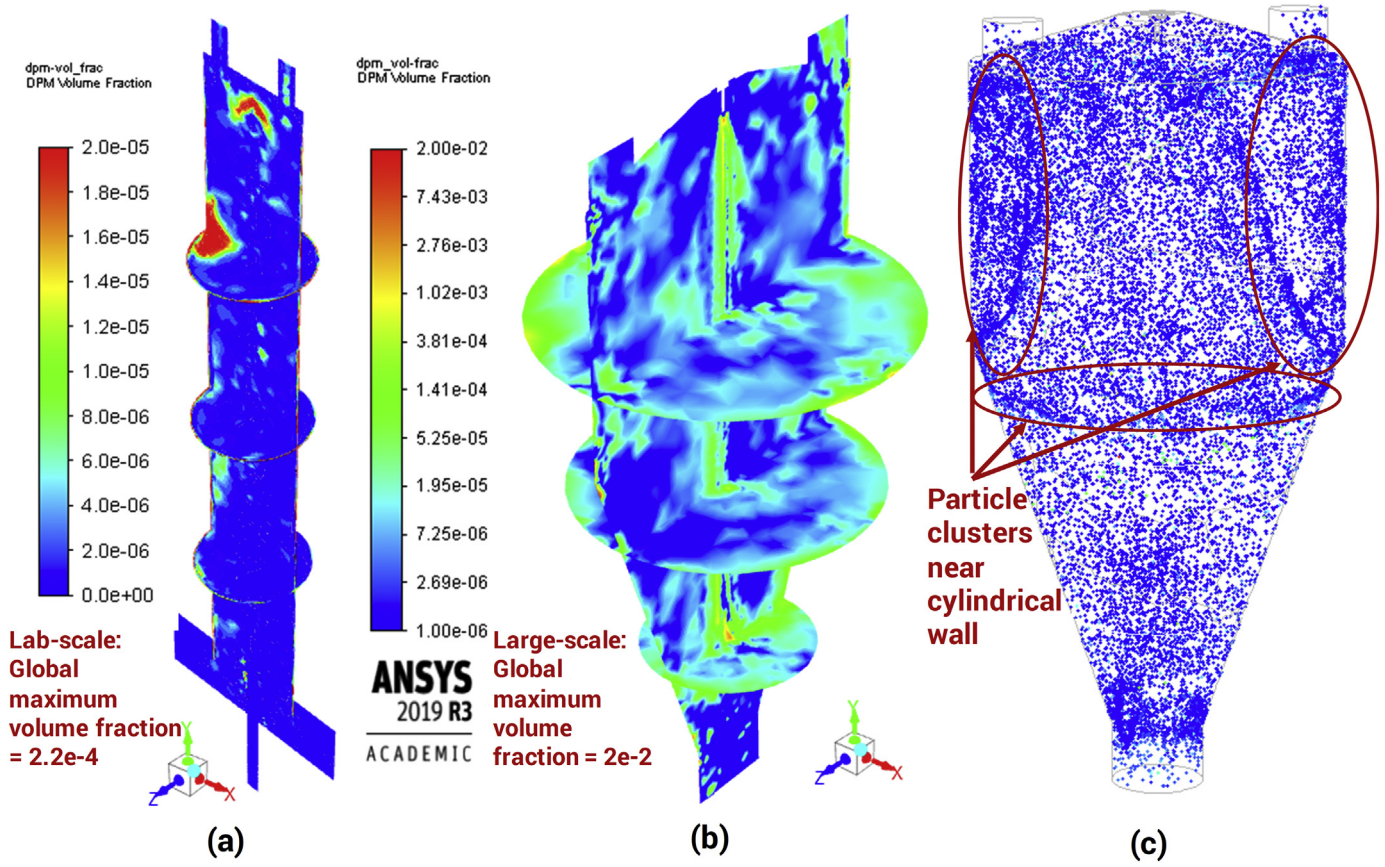

Fig. 10. Contour-plot of volume fraction of the discrete phase (parcel volume fraction) during the simulation run on (a) the lab-scale counter-current spray dryer (configuration Pos2u, Flow-time 120 s), (b) the large-scale spray-dryer (Run1, flow-time 60 s). Scales shown in both colormaps were truncated and adjusted in order to avoid strong contrast and allow optimum representation. (c) Snapshot of tracked particles taken during the simulation of the large-scale spray dryer showing position of the particles within the drying chamber.

fraction of primary particles (not having undergone any coalescence or agglomeration) was negligible, as those particles presumably escaped the dryer through the top air outlet being entrained by the drying air.

The next part of this discussion is dedicated to further evaluating if the reduced agglomerate surface parameter (for detailed description please refer to [35]) can be implemented and used to clearly distinguish different agglomerate structures in a CFD simulation. The reduction in surface area was analyzed to gain some insights into the extent of agglomeration. On this note, it should be mentioned that with successive agglomerations, the maximum possible surface area continues to increase, while the actual agglomerate surface area continues to increase at a lower rate due to partial penetration, and as a result A_{agg}/A_{max}, continues to become smaller. Moreover, for an identical number of agglomerations, a lower value of A_{agg}/A_{max} indicates more compact agglomerate, as the agglomerate surface area continues to decrease with increasing penetration depth.

The distribution of mass undergoing all the collision outcomes that lead to size enlargements is represented as a function of the surface area reduction in Fig. 9a. It can be seen that Pos1 led to the highest fraction of mass (almost 75%) among all configurations corresponding to the extremely small A_{agg}/A_{max} values close to zero. This clearly indicates that consecutive coalescence and agglomeration in this configuration led to most compact conglomerates overall. In contrast, for Pos3, the cumulative distribution curve lying below those of the other two configurations across fairly the entire spread of A_{agg}/A_{max} shows that Pos3 led to the least reduction in surface area. Moreover, Pos3 exhibited slightly higher fraction of less compact particles in the region of A_{agg}/A_{max} values between 0.6 and 1 than the fractions found for the other two configurations. This is manifested by the slightly steeper gradient of the Pos3 curve in the region mentioned. Lying in between the curves of Pos1 and Pos3, the distribution for Pos2u suggests that it led to less fraction undergoing consecutive coalescence and agglomeration than that found with Pos1. Additionally, it indicates that less fraction of loosely attached agglomerates was found for Pos2u than that found for Pos3. Since both coalescence (resulting in spherical particles) and agglomeration (leading to various shapes) may have contributed to this final compactness, the surface area reduction only due to agglomeration was analyzed, in order to deduce further structure related information. This can provide qualitative indication specially pertaining to the extent of penetration of the participating primary particles while the agglomerates are formed.

Analyzing the agglomerates only, Fig. 9b shows the cumulative distribution of agglomerates in terms of different classes of compactness. As can be seen from the figure Pos2u had higher fractions of agglomerates in the comparatively compacter classes of A_{agg}/A_{max} values, by comparison to Pos 1 and Pos3. Due to the absence of any agglomerate compacter than that showing an A_{agg}/A_{max} value of 0.75, all the curves started at a similar level. However, in the sample of Pos2u, as compared to the other runs, the higher rise in cumulative distribution curve up to 0.924 followed by the drop in the rise supported the presence of more compact agglomerates.

The compactness distribution found for Pos1 showed that up to the A_{agg}/A_{max} value of 0.85, the fractions of agglomerates in the compactness classes were fairly similar to those of Pos3. These similar fractions may have occurred due to primary agglomeration i.e. agglomerates consisting of collision partners from the same atomizations. The difference between these two runs were observed for the region lying between 0.85 and 1 i.e. towards the region of less compact agglomerates. For Pos 1 relatively high wetness was expected of the collision partners.

In contrast, Pos3 exhibited significantly lower frequencies in all classes across the compact ranges and surpassed with the rate of increase both Pos1 and Pos2u in the region above 0.925. The sharpest increase in this particular region (loosely attached agglomerate region) clearly indicates that the agglomerates formed during the run Pos3 were mostly due to agglomerations between virtually dried collision partners, where the penetration depth could not reach any higher extent before being stopped by the viscous force of the collector particle. This is expected of Pos3, as the distance between the primary and secondary atomizations was the highest of all and hence the likelihood of more dried particles colliding into each other was higher. Obviously, primary agglomeration also occurred among the particles stemming from the same atomization, but it was the secondary agglomerations that made a noticeable difference.

3.2. Simulations of large-scale spray drying

As can be seen from Fig. 11a, the model which was able to predict the final PSD of the powder sample for the lab-scale spray dryer, markedly overpredicted the final PSD of the powder samples for large-scale dryer. To clarify this, the contour-plots of the mean discrete phase volume fraction found after the simulation runs on both lab- and large-scale spray dryers are shown in Fig. 10a and b respectively. It is noteworthy that the volume fraction of the discrete phase represents the local particle concentration. As can be clearly seen from the plots, the particle number density in the large-scale spray dryer overall is markedly higher by order of magnitudes when compared to that in the lab-scale dryer (see accompanying colormaps). The maximum volume fraction for the large-scale dryer (0.02) was found to be approximately 100 times larger than that found for the lab-scale dryer.

In addition, in both spray dryers the locations were different, at which particularly high concentrations of particles were found. For the lab-scale dryer the relatively high particle concentration was found mostly at and around the atomizations. By contrast, for the large-scale dryer very high particle concentrations were found at the near wall-region, at the location adjacent to the static-fluidized bed in addition to the atomization region. It was suspected that occurrence of these high particle densities was the main reason for multiple consecutive coalescence and agglomeration during the simulation, which led to the significant overprediction in case of the large-scale spray dryer. In our previous study conducted on the same spray dryer [37], we discussed the particle trajectories in detail and suggested that the distinct flow patterns within the chamber led to the formation of particle clusters. In both studies i.e. previous and current, the particle clusters were most commonly found at regions close to the cylindrical wall (see Fig. 10c). Further examination of the surface reduction plots (see Fig. 12b) revealed that the agglomerates had an excessively high extent of consecutive coalescence, and agglomeration, which led to a very high fraction of the agglomerate mass having very small values of A_{agg}/A_{max}. This provides more evidence that these large agglomerates are formed by the agglomeration among an extraordinarily large number of collision partners that are detected most likely at the wall region or the static fluid bed region.

The occurrence of excessively large particles was observed (it should be noted that the observation in question was undertaken only during numerical exploration via CFD simulations, as experimental observation was not possible due to limited access to the interior of the dryer) only in the case of the large-scale spray dryer and not in the lab-scale unit used to initially validate the model. To investigate this phenomenon, the collision routine was bypassed at regions of within 10 cm of the cylindrical wall and at the region adjacent to the fluidized bed (below the sampling plane shown in Fig. 10).

Examining the distribution of the reduced surface area (see Fig. 12b) showed that the extent of consecutive coalescence and agglomeration in the simulation was significantly reduced by the imposed restriction leading to a wider spread of the values for A_{agg}/A_{max}. Nevertheless, while this restriction led to significant improvement of the prediction of particle sizes, the model still overpredicted the particle size distribution leading to non-realistic particle size in the order of 1000 μm (see Fig. 11a). This was an indication that the O'Rourke collision detection scheme may be detecting too many potential collisions for the particle number density encountered in the large-scale spray dryer.

As a basis to further evaluate this, the simulations were repeated to allow the lowest possible number of stochastic particle collision detection. This was undertaken by allowing only the first detected collision instead of letting the routine loop through all particles in the computational cell. In other words, the loop was broken immediately after the first neighboring particle i.e. potential collision partner was detected.

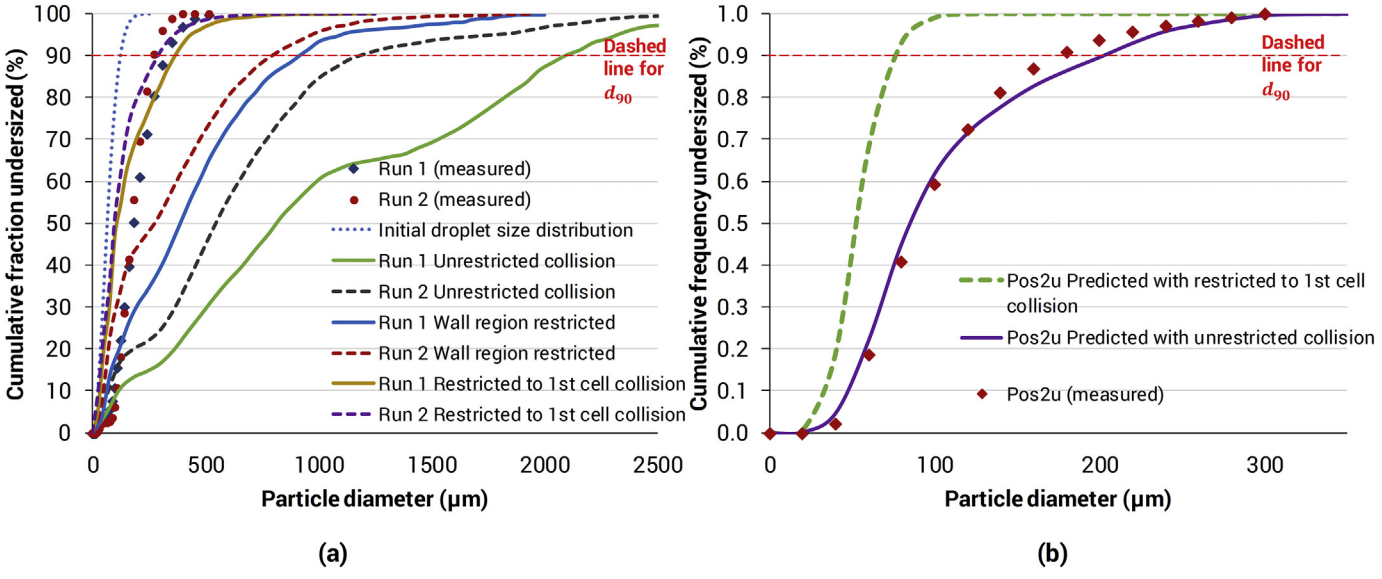

Fig. 11. (a) Comparison between the measured and predicted particle size distributions of the powder samples collected from both outlets of the large-scale spray dryer for both trials. The predictions were taken for comparison from simulation runs with unrestricted collisions, restricted collisions in the wall region and collision restricted to the first detected collision partner in the computational cell. All powder samples were collected for 60 s flow-time. (b) Demonstration of the effect of restricting the collisions to the first detected partner in one computational cell on the prediction of final PSD of the lab-scale spray dryer.

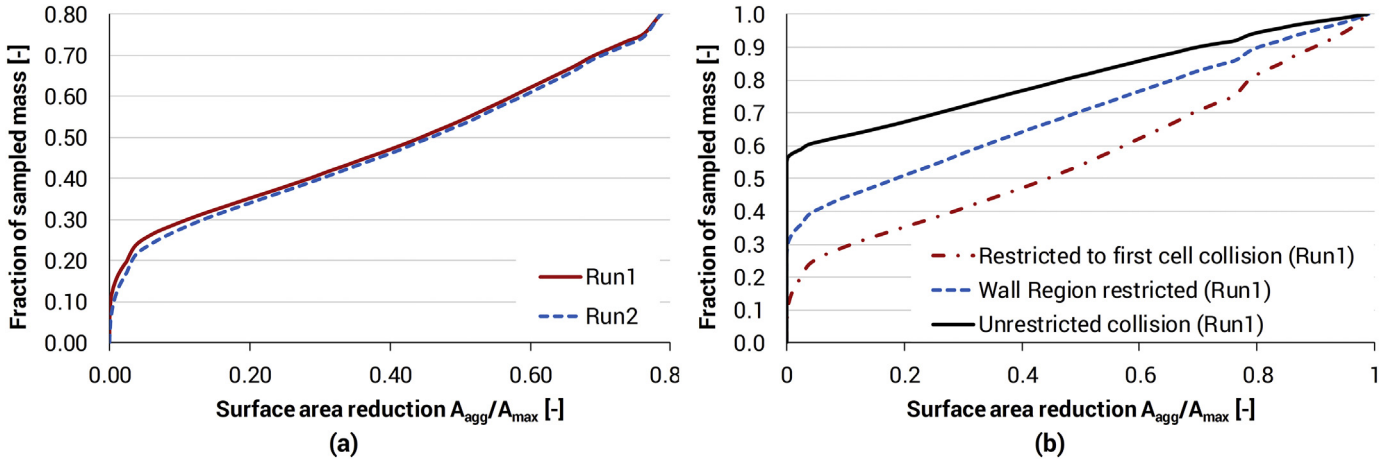

Fig. 12. Comparison of the predicted cumulative distribution of the size enlarged mass as a function of the surface area reduction due to both coalescence and agglomeration among the (a) two runs with restricted collision to the first contact, (b) different approaches with and without collision restrictions implemented for Run1. The analyzed powder samples were collected during CFD simulations at both outlets of the large-scale spray dryer for 60 s.

This measure led to an underprediction of the particle size (see Fig. 11a), particularly for 70% of the mass, which is not unexpected. Investigating the distribution of the reduced surface area (see Fig. 12b) it was found that this measure had greatly reduced the consecutive coalescence and agglomeration so that roughly 10% of the numerically sampled mass showed extremely low (close to zero) values for A_{agg}/A_{max} in place of around 30% found with wall region restricted simulation run. As a result, the mass frequency distribution (not shown here) with respect to A_{agg}/A_{max} of the former showed a flatter and comparatively wider curve, when compared to the latter. To be more specific, analyzing the cumulative distributions it was found that 53% of the size-enlarged mass showed a surface area reduction lower than 0.5 for predictions with first detected collision only, as compared to 70% and 80% for simulation runs with restrictions in wall region and unrestricted collisions respectively. Thus, all evidence confirmed the fact that the number of collisions being detected by O'Rourke algorithm for the large-scale dryer was too high and definitely causing the overprediction of final PSD. The measured data were lying between the lowest predicted PSD with one collision and the improved PSD with the restricted collision in the wall region.

In order to better understand the effect of restricting the collision predictions to the first detected collision partner on a smaller scale dryer, the same method without changing any other parameter was applied to the lab-scale spray dryer reported in the earlier Section 3.1. From Fig. 11b it is evident that, for the lab-scale dryer as well, this method leads to a marked underprediction of the final PSD, as expected. Interestingly, it can be seen that impact of this restriction is significantly more pronounced in the large-scale dryer. This can be quantitatively assessed by evaluating the shifting of the d_{90} i.e. the diameter size, under which 90% of the sample fraction lies. In contrast to the lab-scale dryer where the d_{90} decreased as a result of this applied method by roughly a factor of 2 (from 200 μm to 76 μm), for the large-scale dryer the d_{90} was reduced by more than an order of magnitude.

It is nonetheless noteworthy, that with all three variants our proposed model for collision outcome could predict the observed trend i.e. the Run1 led to a significantly higher particle size than Run2. It can be assumed that in Run2 the lower drying temperature allowed for a slower drying and hence more opportunities to form agglomerates, whereas slightly higher residence time due to lower air velocities in Run 1 led to more opportunities to achieve consecutive coalescence and agglomeration and thus led to higher particle size altogether. This theory was also supported by the distribution of size enlarged mass shown in Fig. 12a, which shows that the distribution of A_{agg}/A_{max} across the range was fairly similar for both runs, except for the initial region, where Run1 exhibited a higher fraction. This higher fraction at very low A_{agg}/A_{max} value must have resulted from higher number of consecutive coalescence and agglomeration, which has contributed to yielding larger particle sizes in Run1.

Despite the overprediction of particle sizes and challenges faced in the simulation of the large-scale spray dryer, the proposed model was able to reveal other important information regarding the extent of agglomeration. When the distribution of the surface area reduction only due to agglomeration was plotted (see Fig. 13), no significant differences was found in agglomerate compactness between the two runs over the majority of the range, except for the range above 0.8. For instance, roughly 25% agglomerated mass in Run 2 showed a surface area reduction of less than 0.90, in contrast to only around 10% of the agglomerated mass for Run 1. This indicates that Run 1 led to slightly higher fraction in loosely attached agglomerates (referring to the sharper rise of fraction beyond the A_{agg}/A_{max} value of 0.90). This along with the significantly larger particle sizes for Run 1 could provide plausible explanations to the bulk and tapped density measurements conducted on the powder samples. The bulk and tapped density of the powder samples from Run1 were measured to be 364.4 kg/m^3 and 432 kg/m^3 respectively. In contrast, the same measurements on the

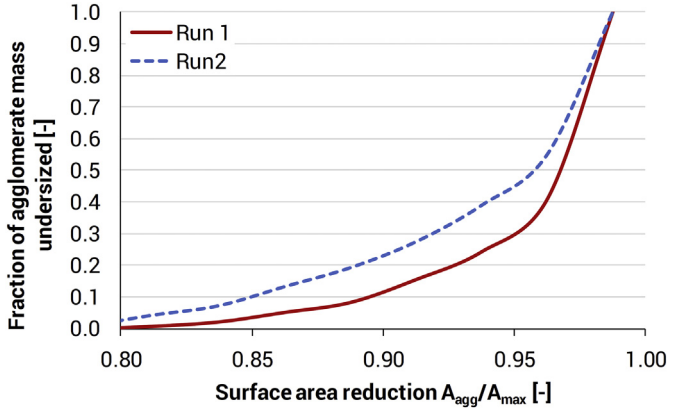

Fig. 13. Representation of the predicted distribution of the agglomerated mass as a function of the surface area reduction due to agglomeration only (excluding coalescence) demonstrating the extent of agglomeration among the two runs. The analyzed powder samples were collected during CFD simulations with collisions restricted to the first contact at both outlets of the large-scale spray dryer for 60 s flow time.

sample from Run 2 showed values of 396.2 kg/m^3 and 457 kg/m^3. Based on the hypothesis that less compact agglomerate and larger particles would lead to more irregular packing allowing for more occluded air and thus decrease both densities, it can be assumed that the comparatively fewer compact agglomerates alongside the larger particle size distribution predicted for Run 1 contributed to the lower bulk and tapped density measured.

In our representation and comparison of the PSD in the figures, for predicted data we have numerically collected the samples in the CFD simulations at the location above the static fluidized bed (see Fig. 10). Since it is well established that the traditional CFD cannot reliably predict the dynamics of the particles within a fluidized bed, we have not attempted to model the fluidized bed as well. Andrews and O'Rourke [43] regarded Lagrangian framework unsuitable for discrete phase volume fraction above 5%. Since it is a small part of the dryer, we deemed the discrepancy owing to the dynamics of the fluidized bed would not alter the trend of the final predictions. Nevertheless, the unmodelled bed may have significantly contributed to the discrepancy observed between the measured and predicted PSD. For instance, it is well expected that further agglomeration and breakage of already enlarged particles due to mechanical stress within the bed would lead to significant deviation in the final PSD. In particular, breakage of large particles would shift the PSD altogether towards left and fines getting attached to sticky particles would result in the opposite effect. Nevertheless, it must be mentioned that the purpose of the work was not to exactly match the experimental data, rather to understand and find the usefulness and drawbacks of the model. While more resources could always be spent on employing further complicated measures such as using MP-PIC method or combining discrete element method (DEM) and traditional CFD to better capture the fluidized bed, the focus of our work was to achieve useful predictions showing at least the correct trend by using minimum resources. It is noteworthy that collisions in Lagrangian particle tracking is considered as an instantaneous phenomenon, whereas in DEM type of calculation scheme, the collision is tracked throughout, an aspect that substantially adds to the numerical requirements. Besides, the other important objective was to establish the usefulness of the proposed model for collision outcomes, which was successfully achieved, since it was proved that the discrepancies are clearly resulting from the underlying collision prediction routine. The limitations of the algorithm as discussed are well-established. However, improving that submodel falls beyond the scope of this study. Nevertheless, as these aspects were identified clearly, these will need to be considered in future works encountering such high particle number density.

3.3. Effect of discrete phase time step size and mesh densities on the final PSD

One of the very interesting research questions was to find out the sensitivity of the final PSD of the powder sample with respect to the time step size employed in the discrete phase calculations. Finding the answer to this question is useful for practical reasons, because lowering

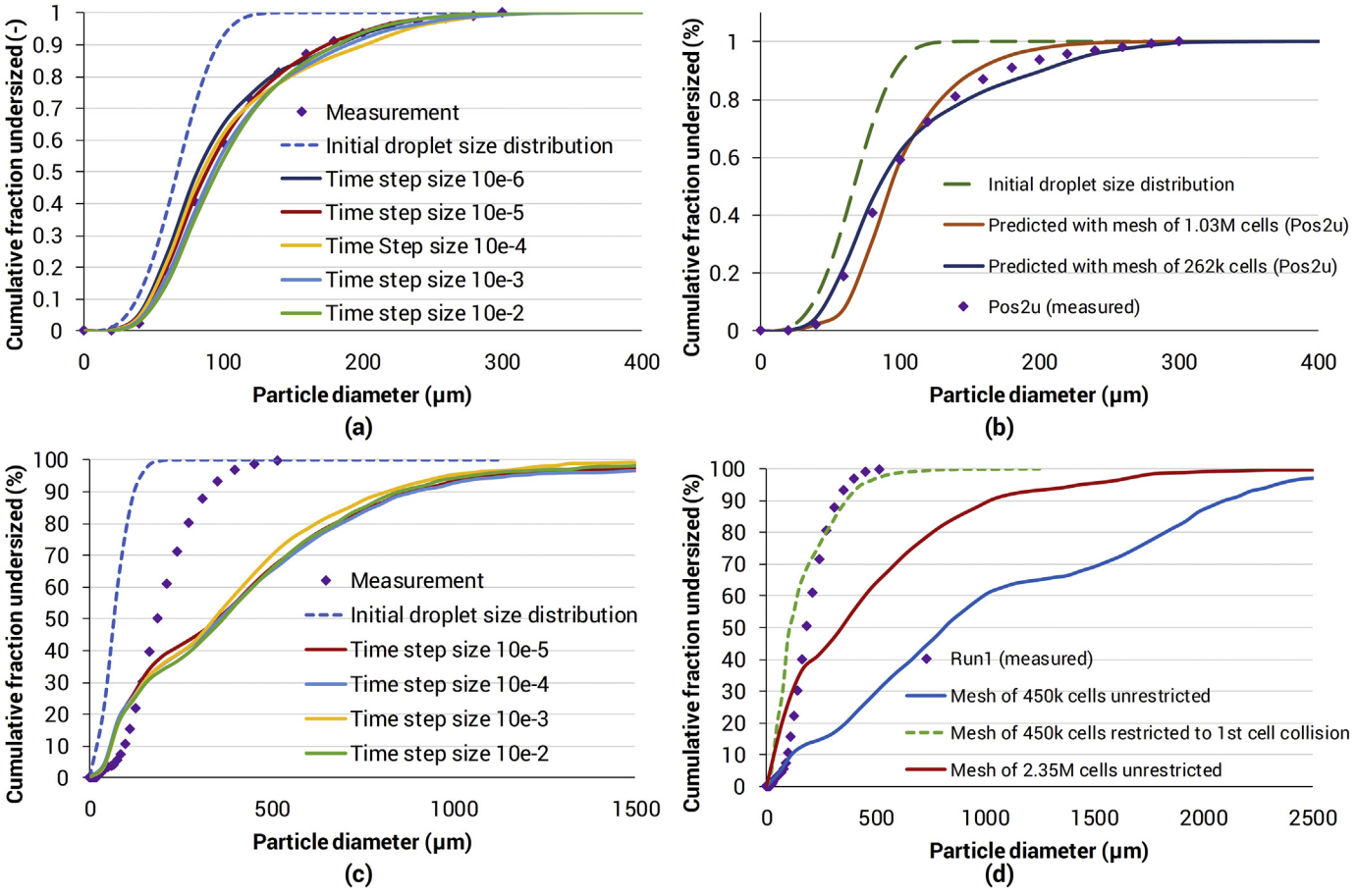

Fig. 14. Demonstration of the effect of time step sizes and computational cell size on the final prediction of particle size distribution. Comparison of the predictions obtained from simulations conducted on the lab-scale spray dryer – shown in (a) — as well as large-scale spray dryer – shown in (c) — with various discrete phase time step sizes. Additionally, comparison of the predictions obtained from simulations with two significantly different grids conducted on the lab-scale spray dryer – shown in (b) — and large-scale spray dryer – shown in (d).

the time step size means accordingly higher number of calculations are necessary in solving the DPM and hence the required computational resources increases. While it is obvious that smaller time step size may lead to higher accuracy and numerical stability, it leads to substantial increase in computational requirements. Therefore, in other words, if the bulk final properties are of main interest, choosing the time step size wisely holds the potential to save substantial amount of time and resources required for simulations.

In general, the time step size needs to be small enough to adequately resolve the mean free path, i.e. the distance travelled by the particles between collisions. In other words, it must be small enough to allow no more than one collision for one particle within one time step. In the traditional DSMC method time step is a constant value. If we review the collision routine, we can clearly see that according to Eq. (2) the collision volume and thus the collision probability may increase with the increase in time step size. This may lead to increased collision frequency and thus possibly higher size enlargement. At the same time, an increase in the collision probability due a longer time step may be partially offset by a reduction in the number of time steps required for the simulation of identical flow time simulation. Presumably these two opposing effects would not cancel each other out leaving a combined result. Moreover, the final PSD is dependent on so many other variables such as drying history and particle trajectory calculations that the impact on the PSD may not be as straight-forward. For instance, if drying is overpredicted due to large time step size, the stickiness of the particle may decrease and thus the collision outcome may not be a coalescence or agglomeration after all. Similarly, due to overprediction of drag force via larger time step the collision outcome may as well be different. The counteracting effects may nullify each other to some extent leading to an insignificant difference in the final PSD. This was virtually the case, when the same simulation was performed with different time step sizes. Despite varying the time step by one order of magnitude size starting from 10^{-2} (5 times smaller than the fluid phase time step size i.e. 0.05 s) up to 10^{-6} (50,000 times smaller than the fluid phase time step size), the final predicted PSD's were not found to be significantly different (see Fig. 14a). Same findings were affirmed for the simulations performed with large size dryer (see Fig. 14c) for time step sizes ranging between 10^{-2} and 10^{-5} s. For both cases the time step size 10^{-2} led to a slightly higher deviation, which can be attributed to the less accurate resolution in prediction of drying history and trajectories. As a result, it was concluded that for the simulations conducted for this work the employed time step size 10^{-4} s was sufficiently fine and had no significant impact in the observed overprediction of the PSD. Nevertheless, it must be noted that the prediction of PSD is not in general independent of time step size, it was only found to be insensitive to the time steps lying in the tested ranges, since the time step size was sufficiently small. For future similar simulation works, 10^{-3} s is recommended, which could save substantial amount of computational resources, unless methods involving adaptive time step is employed. For instance, Du, Zhao, Zhou, Guo and Hao [59] suggested an alternative DSMC method, which calculates the mean free path in every time step and adapts its size accordingly. We decided not to employ this method, as choosing a sufficiently small constant time step size saves the resources required to complete the calculations for adaptation. Besides, in simulation of spray drying in addition to the mean free path, the potential impacts of the time step size on other submodels such as drying and drag calculations must be considered.

Finally, it was of great interest to check the well-known mesh dependence of O'Rourke algorithm, which has already been mentioned earlier. In order to better investigate the effect, we first chose the large-scale dryer, for which the issue of overprediction was already being observed. The overpredicted PSD led to the suspicion that the cell sizes in the grid may be too large and are leading to markedly higher number of particles to be considered as collision partners, even though for the flow field predictions the mesh dependence was already established. Therefore, we have employed another mesh consisting of roughly 2.35 million cells as compared to the primarily used mesh consisting of approximately 450,000 cells. As can be seen from Fig. 14d, we could confirm that with higher mesh density the collision frequency and subsequently the particle enlargement could be significantly decreased. However, even with the fairly fine mesh, the overprediction of the PSD could not be avoided. It was also demonstrated in the same graph that as expected, with higher number of cells the PSD prediction would gradually approach that determined with the method of restricting the collision to the first collision partner in the computational cell applied on a coarser mesh, which can be deemed the minimum possible PSD of all. This test also confirms that the major reason behind the overprediction of the final PSD for the large-scale spray dryer was the routine for collision detection and not that of the collision outcome model.

Finally, to understand the effect of a much denser mesh on the predictions achieved for the lab-scale dryer, we have replaced our already established mesh of approximately 262,000 cells with one consisting of roughly 1.03 million cells. The results are shown in Fig. 14b, which again shows that the PSD shifts to the left as well in case of the lab-scale dryer leading to a higher fraction of fines and lower fractions of large particles. This obviously results from the smaller number of particles available for collision in the much finer mesh with smaller cells. However, it was interesting to observe that the effect of mesh dependence is not as pronounced as in case of the large-scale dryer. This implies that with O'Rourke's collision detection routine, finding an appropriate mesh becomes much more important with increasing number density of particles or the volume fraction of the discrete phase.

Hence, we argue that the performance of the method depends on the mesh as well as on the scale of the equipment. It is possible to design meshes that give better performance for the large-scale dyer. To this end, by taking the size of the computational cells as a baseline requirement that denotes the overall performance of the model, the most straightforward approach could be to reduce the size of the cells of the large-scale dryer to match that of the small-scale dryer. Logically, such an approach should involve selective mesh adaptation, as an overall mesh size reduction across the computational domain is unlikely to be practical. Perhaps the number density of particles could be utilized as a parameter governing the adaptation. Nevertheless, to the best of authors' knowledge, no such agglomeration based selective transient mesh adaptation scheme is available in the literature. In any case, the mesh adaptation will inevitably increase the computational requirements for the simulation, which will be further compounded by the transient nature of the simulation.

3.4. Derivation of areas and pertaining studies for future work by highlighting the limitations of the used model

Among the limitations listed in Section 2.2.4 and, the most significant one is the intrinsic mesh dependence of the model (also shown in Section 3.3), which stems from the assumption that only those particles currently located in the same cell as the tracked particle are considered as collision partner. This means even though two parcels were located fairly close to each other i.e. within a distance prone to collision however not in the identical computational cell, they would yet not end up colliding into each other. It must be conceded that considering some parcels located farther apart in a larger cell for collision counteracts the error caused in smaller cells. In general, excessively fine meshes could lead to significantly lower number of collisions predicted than that actually occurring, whereas coarse meshes could lead to higher number of collisions. If a fine mesh is absolutely necessary to accurately capture the flow field features, we suggest that the adjacent cells to the current computational cells are included in the calculation. This was not necessary in the investigated cases; however, we have nonetheless

implemented the suggestion by making necessary adjustments to the UDF and run comprehensive tests. We could conclude that this significantly increase the number of collisions experienced by the tracked particles and hence can be used as a feasible method to improve given the abovementioned issue. As an alternative approach we also implemented the idea of defining a collision volume first and then considering the particles located within that volume for potential collisions (similar concept as was reported by Zhang, Mi and Wang [23]). However, this probing approach proved considerably more resource intensive than the original approach of limiting within one or multiple cells, since under the current calculation scheme of the commercial package ANSYS Fluent for each tracked particle the routine is required to loop through all tracked particles in the domain to find the eligible candidates. To the best of our knowledge, currently there exists no efficient method in the traditional DPM of limiting the search for collision partner only within a defined distance without checking through each and every particle in the domain. In contrast to approximately a minute required by our approach for the calculation of each time step for a fully developed simulation (with around 40,000 parcels in the domain) of the lab-scale dryer, the searching through the entire domain approach took more than 2 h to finish each fluid flow time step. Thus, the later approach was found to be unsuitable for large-scale simulations. Of course, this can be revisited, once some alternative way of limiting the search is discovered. For instance, as an alternative avenue to be explored could be a method used in DEM of dividing the domain by a suitable cartesian mesh for evaluating collision, where the edge length is defined as a function of the particle diameters [57]. At any rate, the achieved accuracy by the first approach was found to be reasonable and hence this approach was deemed suitable and effective considering the required computational resources.

The model for impact efficiency was adapted from the original model developed to describe the fine dust particles being separated from a fluid flow through droplets [52,60]. Obviously, the fine dust particles are smaller than the droplet. However, due to the generic description of the model in terms of dimensionless numbers with the empirical constants (function of only collector Reynolds number) being independent of any interrelationship between the sizes, the original model was assumed to be still valid, if the collector particle happened to be smaller than the contributor. Despite the apparent limitation of the model, based on the literature review the implemented method to estimate the impact efficiency was found to be the most suitable one for agglomeration modeling in the employed framework. While developing a novel more accurate model for impact efficiency lies beyond the scope of this work, the objective of this attempt was merely to propose a possibility as to how this specific concept of impact efficiency could be integrated in the proposed agglomeration model. If a more suitable model can be developed, the identical interface can be utilized for implementation.

As for the drag calculation, instead of capturing the motion of a potentially nonspherical particle/droplet that eventually partially penetrates or fully merge with another droplet/particle resulting in an agglomerate or coalesced particle of diverse shapes, the proposed model still assumes the motion of a solid sphere through an infinite fluid. In order for this simplification to be discarded, the prerequisite would be the detailed information about the structure of the particles. While our proposed model was able to provide indications as to the particle/agglomerate compactness, the exact shape and structure of the particles could not be stored mainly constrained by the goal of saving computational resources. Moving away from the usual assumption of spherical particles, if the agglomerate structure can be predicted with additional details, the drag calculation model can then be easily adapted as well. This may lead to substantial improvement in predicting the particle trajectories. In support of this idea, while studying the fluid dynamic behavior of different agglomerate structures, Stübing, Dietzel and Sommerfeld [33] concluded that the widely used volume equivalent sphere was unsuitable for Lagrangian tracking. The equivalent diameter of the convex hull closely representing the agglomerate was recommended instead. A review of literature has revealed a number of studies developing various drag models for regular and irregular shapes [61–66]. However, none of the CFD-studies of spray drying has hitherto incorporated a different drag model other than that applicable to spheres. However, we strongly recommend that as soon as the resulting particle shape can be predicted and stored in a full scale CFD spray drying simulation, an appropriate drag model should be implemented to improve the accuracy of the predictions pertaining to particle motion. This improvement will inevitably affect the predictions of the drying history as well as the final PSD.

Furthermore, in a recently published series of works [11,16,67] droplet-droplet collision interactions were investigated both experimentally and numerically using DSMC approach in Eulerian-Lagrangian framework. While the series of work provided vital insights into the collision dynamics and the impacts of various process parameters on the collision outcomes as well as the effect of the collisions on the continuous phase, the main focus was put on the distinction among coalescence, bouncing and separation of droplets ignoring agglomeration of sticky particles. It was shown, by including the stretching and reflexive separation of droplets in determining the collision outcomes in a spray of different fluids including water and milk, that the percentage of separation ranged between 34.7% and 66.1%, whereas coalescence ranged from 29.6% to 54.1% within 0.3 s of simulation time [67]. Bai [68] also compared simulation results and showed that particle size can be significantly overpredicted with permanent coalescence assumed to be the only collision outcome and ignoring the breakup processes. Thus, it becomes evident that with reference to coalescence, separation of droplets forming satellite droplets, is not negligible. Including this phenomenon in modeling the collision outcome would subsequently further reduce the predicted PSD of the final powder and would help match the experimental data.

4. Conclusions

In this study, a new agglomeration model based on O'Rourke collision algorithm [21] for Eulerian-Lagrangian framework has been proposed. The model was used to perform complete transient CFD-simulations of spray drying of skim milk in both lab-scale and large-scale. Experimental data were utilized to verify the model as well as to support the interpretation and analysis of the simulation results.

The purpose of the new developments in the collision model was to distinguishing between agglomeration and coalescence as collision outcomes and preserve as much structure related information as possible. Our proposed model was implemented to determine and utilize the penetration depth during formation of agglomerates, based on viscous dissipation of momentum. Additionally, the penetration depth was used to calculate and store the surface area equivalent diameter for further treatment of the newly formed agglomerate. The reduction in surface area as well as the decided collision fate were stored in particle memory and used to further derive information about the compactness of agglomerates. This enabled us to understand and establish the formation of compact or loose agglomerates. It was found that the new agglomeration model can clearly distinguish realistic differences in agglomerate structures. This was confirmed for the small scale and the large-scale spray dryers. The findings from the analysis of the simulation results agreed with the experimental evidence.

For lab-scale counter-current dryer simulations, size enlargements occurred could be accurately predicted. Furthermore, for the first time, from simulations performed with spherical equivalent particles, the collision outcomes of coalescence and agglomeration could be clearly distinguished, and the compactness of the agglomerates could be delineated. As a result, the differences in particle size as well as extent of agglomeration among different runs could be successfully resolved.

For large-scale dryer simulations, the trend in particle size enlargement was correctly predicted, but the estimation of particle sizes was clearly overpredicted. This overprediction resulted from the inherent mesh dependence as well as a limitation of the underlying collision detection routine for high particle number densities. Measures were implemented to counteract these limitations including restricting the zone with high volume fraction (based on the observed particle clusters forming at the cylindrical wall region) and restricting the collision to the first detected collision partner inside the computational cell. When these measures were used, the prediction of particle sizes improved. Additionally, these measures enabled the underlying cause behind the overshoot to be clearly understood and established. The measures would also be useful, if one must use the current version of the model in prediction of agglomeration in large-scale dryers with high particle number densities, due to lack of available resources or further development. Despite the overpredictions, the newly introduced parameter of surface area reduction due to agglomeration in the proposed model could provide valuable information about the particle structures e.g. the compactness of the resulting agglomerates. Experimental evidence of measured PSD and bulk densities corroborated this deduced indication related to the agglomerate compactness combined with the predicted trend in PSD.

Based on the findings obtained from the investigation of the large-scale dryer, it is recommended that the proposed model should be tuned to a particular piece of equipment as well as a particular mesh. Experimental data will be necessary to perform such tuning until the problem of the inherent mesh dependence of the collision detection routine is solved by any future endeavor. In the setting up the CFD model, after the mesh independence of the flow field calculations is established, the predicted discrete phase properties such as PSD, moisture content and agglomerate structures must be compared with the experimental observations. If the discrepancy is deemed too great, further refining of the mesh needs to be undertaken. This work also identifies a number of different ways to tune the proposed model for use in practical applications.

This work has also clearly identified the areas that deserve further attention. Apart from overcoming the inherent mesh dependence of the O'Rourke collision detection algorithm, it became clear that the stretching and reflexive separation of droplets should be included as possible collision outcomes. In addition, dry particle agglomeration due to cohesive force and breakage of particles should be incorporated in the model, in order to achieve a more accurate collision model for spray drying applications. However, such amendments to the collision routine can be easily added on to the new developments of the proposed model.

In summary, this work not only provides a further step towards achieving CFD models, which can be utilized to predict final powder properties, it also provides a useful tool for industry as well as the scientific community that can be used to understand, design and control agglomeration, without demanding the computational resources of a prohibitive high-performance computing (HPC).

Notation

Latin letter

a	intersection length between overlapping particles/droplets (m^2)
a_1, a_2	model coefficients (m^2)
A	surface area (m^2)
b	factor in linear shrinkage model/offset parameter in O'Rourke model (−)
d	diameter (−)
f	factor (−)
h	penetration depth during collision between droplets/particles (m)
m	mass (kg)
n	number of droplets (−)
N	number of collisions (−)
P	probability (−)
r	relative distance between collision partners (m)
Re	Reynolds number (−)
St	Stokes number (−)
t	time (s)
v	velocity (m/s)
V	volume (m^3)
We	Weber number (−)
x	mass fraction (−)
X	dry basis moisture content (kg H_2O/kg solid)
Y	randomly generated number (−)
Z	reduction in surface area/ratio of agglomerate to maximum surface area (−)

Greek letter

Δ	difference (−)
μ	dynamic viscosity (kg/m/s)
η	efficiency (−)
ρ	density (kg/m)
σ	surface tension (N/m)

Subscripts

0	initial
agg	agglomerate
col	collision
cont	contact
cr	critical
eq	equivalent
m	mass
max	maximum
p	particle
ref	reference
rel	relative

Declaration of competing interest

The authors declare that they have no known competing financial interests or personal relationships that could have appeared to influence the work reported in this paper.

Acknowledgements

The first author acknowledges the support provided by the Australian Government Department of Industry, Innovation, and Science through the Australia-China Science and Research Fund (ACSRF48154), as part of the research program of the Australia-China Joint Research Centre in Future Dairy Manufacturing (http://acjrc.eng.monash.edu/). Moreover, the use of facilities within the Monash Centre for Electron Microscopy (MCEM) is gratefully acknowledged. The first author owes a debt of gratitude to Ms. Jane Moodie and Dr. Lilian Khaw for their invaluable feedback on the manuscript. Furthermore, the personal communication with and the invaluable assistance provided by the Development Team Leader of ANSYS Germany GmbH, Dr.-Ing. Markus Braun was crucial to the accomplishment of this study. Soochow University acknowledges The National Key Research and Development Program of China (International S&T Cooperation Program, ISTCP, 2016YFE0101200) for support of the Australia-China collaboration. Furthermore, the second author acknowledges the support provided by VESKI (Victorian Endowment for Science, Knowledge and Innovation). The VESKI fellowship award enabled her visit to INRA (French National Institute for Agricultural Research in Rennes, France) and thus

facilitated under the collaboration between Monash University and INRA the crucial experimental trials on the large-scale (BIONOV) spray dryer to be completed.

Appendix A. Supplementary data

Supplementary data to this article can be found online at https://doi.org/10.1016/j.powtec.2020.05.111.

References

[1] P.S. Hansen, Production of agglomerated fat-filled milk powder, Int. J. Dairy Technol. 33 (1980) 19–23.
[2] T. Retsina, Agglomeration: a process to improve fine powder handling, Food Technology International Europe, Food Technology International Europe 1988, pp. 37–39.
[3] A.M. Williams, J.R. Jones, A.H.J. Paterson, D.L. Pearce, Effect of fines on agglomeration in spray dryers: an experimental study, Int. J. Food Eng. 5 (2009), 7.
[4] S. Chever, S. Méjean, A. Dolivet, F. Mei, C.M. Den Boer, G. Le Barzic, R. Jeantet, P. Schuck, Agglomeration during spray drying: physical and rehydration properties of whole milk/sugar mixture powders, LWT Food Sci. Technol. 83 (2017) 33–41.
[5] R.E.M. Verdurmen, P. Menn, J. Ritzert, S. Blei, G.C.S. Nhumaio, T. Sonne Sørensen, M. Gunsing, J. Straatsma, M. Verschueren, M. Sibeijn, G. Schulte, U. Fritsching, K. Bauckhage, C. Tropea, M. Sommerfeld, A.P. Watkins, A.J. Yule, H. Schønfeldt, Simulation of agglomeration in spray drying installations: the EDECAD project, Dry. Technol. 22 (2004) 1403–1461.
[6] B. Guo, D.F. Fletcher, T.A.G. Langrish, Simulation of the agglomeration in a spray using Lagrangian particle tracking, Appl. Math. Model. 28 (2004) 273–290.
[7] J. Pisecký, Handbook of Milk Powder Manufacture, GEA Process Engineering A/S (GEA Niro), Copenhagen, Denmark, 1997.
[8] I.C. Kemp, D.E. Oakley, Modelling of particulate drying in theory and practice, Dry. Technol. 20 (2002) 1699–1750.
[9] D.E. Oakley, Scale-up of spray dryers with the aid of computational fluid dynamics, Dry. Technol. 12 (1994) 217–233.
[10] J.J. Nijdam, B. Guo, D.F. Fletcher, T.A.G. Langrish, Challenges of simulating droplet coalescence within a spray, Dry. Technol. 22 (2004) 1463–1488.
[11] G. Finotello, R.F. Kooiman, J.T. Padding, K.A. Buist, A. Jongsma, F. Innings, J.A.M. Kuipers, The dynamics of milk droplet–droplet collisions, Exp. Fluids 59 (2017), 17.
[12] I. Zbicinski, X. Li, Conditions for accurate CFD modeling of spray-drying process, Dry. Technol. 24 (2006) 1109–1114.
[13] M. Jaskulski, P. Wawrzyniak, I. Zbiciński, CFD model of particle agglomeration in spray drying, Dry. Technol. 33 (2015) 1971–1980.
[14] M. Sommerfeld, S. Stübing, A novel Lagrangian agglomerate structure model, Powder Technol. 319 (2017) 34–52.
[15] C.A. Ho, M. Sommerfeld, Modelling of micro-particle agglomeration in turbulent flows, Chem. Eng. Sci. 57 (2002) 3073–3084.
[16] G. Finotello, J.T. Padding, K.A. Buist, A. Schijve, A. Jongsma, F. Innings, J.A.M. Kuipers, Numerical investigation of droplet-droplet collisions in a water and milk spray with coupled heat and mass transfer, Dry. Technol. (2019) 1–23.
[17] D.B. Southwell, T.A.G. Langrish, Observations of flow patterns in a spray dryer, Dry. Technol. 18 (2000) 661–685.
[18] S. Sundaram, L.R. Collins, Collision statistics in an isotropic particle-laden turbulent suspension. Part 1. Direct numerical simulations, J. Fluid Mech. 335 (1997) 75–109.
[19] M. Ernst, M. Sommerfeld, On the volume fraction effects of inertial colliding particles in homogeneous isotropic turbulence, J. Fluids Eng. 134 (2012).
[20] N. Almohammed, M. Breuer, Modeling and simulation of agglomeration in turbulent particle-laden flows: a comparison between energy-based and momentum-based agglomeration models, Powder Technol. 294 (2016) 373–402.
[21] P.J. O'Rourke, Collective Drop Effects on Vaporizing Liquid Sprays, Princeton University, Princeton, New Jersey, 1981.
[22] C.T. Crowe, J.D. Schwarzkopf, M. Sommerfeld, Y. Tsuji, Multiphase Flows with Droplets and Particles, Second ed. CRC Press, Boca Raton London New York, 2011.
[23] J. Zhang, J. Mi, H. Wang, A new mesh-independent model for droplet/particle collision, Aerosol Sci. Technol. 46 (2012) 622–630.
[24] Q. Li, T.-m. Cai, G.-q. He, C.-b. Hu, Droplet collision and coalescence model, Appl. Math. Mech. 27 (2006) 67–73.
[25] D.P. Schmidt, C.J. Rutland, A new droplet collision algorithm, J. Comput. Phys. 164 (2000) 62–80.
[26] M. Sommerfeld, Validation of a stochastic Lagrangian modelling approach for inter-particle collisions in homogeneous isotropic turbulence, Int. J. Multiphase Flow 27 (2001) 1829–1858.
[27] M. Mezhericher, A. Levy, I. Borde, Droplet–droplet interactions in spray drying by using 2d computational fluid dynamics, Dry. Technol. 26 (2008) 265–282.
[28] M. Mezhericher, A. Levy, I. Borde, Probabilistic hard-sphere model of binary particle–particle interactions in multiphase flow of spray dryers, Int. J. Multiphase Flow 43 (2012) 22–38.
[29] B.P.B. Hoomans, Granular Dynamics of Gas-Solid Two-Phase Flows, University of Twente, Enschede, Netherlands, 1999 242.
[30] M.J.V. Goldschmidt, Hydrodynamic Modelling of Fluidised Bed Spray Granulation, University of Twente, Enschede, Netherlands, 2001.
[31] S. Blei, M. Sommerfeld, CFD in drying technology – spray-dryer simulation, Modern Drying Technology, Wiley-VCH Verlag GmbH & Co. KGaA 2007, pp. 155–208.
[32] S. Stübing, M. Sommerfeld, Lagrangian modelling of agglomerate structures in a homogeneous isotropic turbulence, 7th International Conference on Multiphase Flow. ICMF2010Tampa, FL USA, 2010.
[33] S. Stübing, M. Dietzel, M. Sommerfeld, Modelling agglomeration and the fluid dynamic behaviour of agglomerates, ASME-JSME-KSME 2011 Joint Fluids Engineering Conference, American Society of Mechanical Engineers 2011, pp. 3257–3267.
[34] S. Stübing, Lagrangesche Berechnung von Agglomeratstrukturen am Beispiel eines Sprühtrockners, Zentrums für Ingenieurwissenschaften, Lehrstuhl Mechanische Verfahrenstechnik, Martin-Luther-Universität Halle-Wittenberg, 2014.
[35] H. Jubaer, R. Dai, E. Ruslim, S. Mansouri, Z. Shan, M.W. Woo, New perspectives on capturing particle agglomerates in CFD modeling of spray dryers, Dry. Technol. 38 (2020) 685–694.
[36] H. Jubaer, J. Xiao, X.D. Chen, C. Selomulya, M.W. Woo, Identification of regions in a spray dryer susceptible to forced agglomeration by CFD simulations, Powder Technol. 346 (2019) 23–37.
[37] H. Jubaer, S. Afshar, G. Le Maout, S. Mejean, C. Selomulya, J. Xiao, X.D. Chen, R. Jeantet, M.W. Woo, The impact of self-sustained oscillations on particle residence time in a commercial scale spray dryer, Powder Technol. 360 (2020) 1177–1191.
[38] G.A. Bird, Approach to translational equilibrium in a rigid sphere gas, Phys. Fluids 6 (1963) 1518–1519.
[39] G.A. Bird, DSMC Procedures in a Homogeneous Gas, Molecular Gas Dynamics and the Direct Simulation of Gas Flows, Oxford University Press, New York, 1994 218–256.
[40] D.P. Schmidt, C.J. Rutland, Reducing grid dependency in droplet collision modeling, J. Eng. Gas Turbines Power 126 (2004) 227–233.
[41] S. Hou, D.P. Schmidt, Adaptive collision meshing and satellite droplet formation in spray simulations, Int. J. Multiphase Flow 32 (2006) 935–956.
[42] G.H. Ko, H.S. Ryou, Droplet collision processes in an inter-spray impingement system, J. Aerosol Sci. 36 (2005) 1300–1321.
[43] M.J. Andrews, P.J. O'Rourke, The multiphase particle-in-cell (MP-PIC) method for dense particulate flows, Int. J. Multiphase Flow 22 (1996) 379–402.
[44] P.J. O'Rourke, P. Zhao, D. Snider, A model for collisional exchange in gas/liquid/solid fluidized beds, Chem. Eng. Sci. 64 (2009) 1784–1797.
[45] P.J. O'Rourke, D.M. Snider, An improved collision damping time for MP-PIC calculations of dense particle flows with applications to polydisperse sedimenting beds and colliding particle jets, Chem. Eng. Sci. 65 (2010) 6014–6028.
[46] P.J. O'Rourke, D.M. Snider, Inclusion of collisional return-to-isotropy in the MP-PIC method, Chem. Eng. Sci. 80 (2012) 39–54.
[47] R.B. Keey, M. Suzuki, On the characteristic drying curve, Int. J. Heat Mass Transf. 17 (1974) 1455–1464.
[48] T.A.G. Langrish, T.K. Kockel, The assessment of a characteristic drying curve for milk powder for use in computational fluid dynamics modelling, Chem. Eng. J. 84 (2001) 69–74.
[49] T.T.H. Tran, M. Jaskulski, E. Tsotsas, Reduction of a model for single droplet drying and application to CFD of skim milk spray drying, Dry. Technol. 35 (2017) 1571–1583.
[50] A. FLUENT, Help System, ANSYS FLUENT Users Guide, Release 2019 R3, ANSYS, Inc., 2019
[51] M. Pinsky, A. Khain, M. Shapiro, Collisions of small drops in a turbulent flow. Part I: collision efficiency. Problem formulation and preliminary results, J. Atmos. Sci. 56 (1999) 2585–2600.
[52] G. Schuch, F. Löffler, Über die Abscheidewahrscheinlichkeit von Feststoffpartikeln an Tropfen in einer Gasströmung durch Trägheitseffekte, Verfahrenstechnik 12 (1978) 302–306.
[53] V. Westergaard, Milk Powder Technology: Evaporation and Spray Drying, GEA Niro A/S, Copenhagen, 2004.
[54] S.X.Q. Lin, X.D. Chen, Changes in milk droplet diameter during drying under constant drying conditions investigated using the glass-filament method, Food Bioprod. Process. 82 (2004) 213–218.
[55] H. Jubaer, S. Afshar, J. Xiao, X.D. Chen, C. Selomulya, M.W. Woo, On the importance of droplet shrinkage in CFD-modeling of spray drying, Dry. Technol. 36 (2018) 1785–1801.
[56] N. Fu, M.W. Woo, C. Selomulya, X.D. Chen, Shrinkage behaviour of skim milk droplets during air drying, J. Food Eng. 116 (2013) 37–44.
[57] ANSYS® FLUENT, Help System, ANSYS FLUENT Theory Guide, Release 2019 R3, ANSYS, Inc., U.S.A., 2019
[58] H. Jubaer, S. Afshar, J. Xiao, X.D. Chen, C. Selomulya, M.W. Woo, On the effect of turbulence models on CFD simulations of a counter-current spray drying process, Chem. Eng. Res. Des. 141 (2019) 592–607.
[59] M. Du, C. Zhao, B. Zhou, H. Guo, Y. Hao, A modified DSMC method for simulating gas–particle two-phase impinging streams, Chem. Eng. Sci. 66 (2011) 4922–4931.
[60] G. Schuch, F. Löffler, Untersuchungen zur Abscheidung von Staubpartikeln aus einer Luftströmung durch Wassertropfen, Chem. Ing. Tech. 51 (1979) 301–302.
[61] A. Haider, O. Levenspiel, Drag coefficient and terminal velocity of spherical and non-spherical particles, Powder Technol. 58 (1989) 63–70.
[62] S. Tran-Cong, M. Gay, E.E. Michaelides, Drag coefficients of irregularly shaped particles, Powder Technol. 139 (2004) 21–32.

[63] A. Hölzer, M. Sommerfeld, New simple correlation formula for the drag coefficient of non-spherical particles, Powder Technol. 184 (2008) 361–365.
[64] E. Loth, Drag of non-spherical solid particles of regular and irregular shape, Powder Technol. 182 (2008) 342–353.
[65] G. Bagheri, C. Bonadonna, On the drag of freely falling non-spherical particles, Powder Technol. 301 (2016) 526–544.
[66] W. Zhong, A. Yu, X. Liu, Z. Tong, H. Zhang, DEM/CFD-DEM modelling of non-spherical particulate systems: theoretical developments and applications, Powder Technol. 302 (2016) 108–152.
[67] G. Finotello, J.T. Padding, K.A. Buist, A. Jongsma, F. Innings, J.A.M. Kuipers, Droplet collisions of water and milk in a spray with Langevin turbulence dispersion, Int. J. Multiphase Flow 114 (2019) 154–167.
[68] C. Bai, Modeling of Spray Impingement Processes, Department of Mechanical Engineering, Imperial College of Science, Technology & Medicine, Imperial College of Science, Technology & Medicine, University of London, London, 1996.